University of Rhode Island

DigitalCommons@URI

1998

Crack Propagation and Damage Mechanics in Particle-Matrix Composites

Thomas Edwin Archibald
University of Rhode Island

Recommended Citation

CRACK PROPAGATION AND DAMAGE MECHANICS

IN PARTICLE-MATRIX COMPOSITES

BY

THOMAS EDWIN ARCHIBALD

A THESIS SUBMITTED IN PARTIAL FULFILLMENT OF THE

REQUIREMENTS FOR THE DEGREE OF

MASTER OF SCIENCE

IN

MECHANICAL ENGINEERING AND APPLIED MECHANICS

UNIVERSITY OF RHODE ISLAND

1998

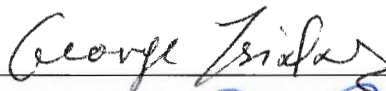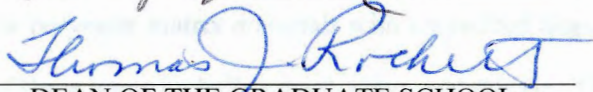MASTER OF SCIENCE THESIS

OF

THOMAS EDWIN ARCHIBALD

APPROVED:

Thesis Committee

Major Professor

DEAN OF THE GRADUATE SCHOOL

UNIVERSITY OF RHODE ISLAND

1998

ABSTRACT

A search of the literature has shown that a large number of empirical models exist for predicting the fracture toughness of particle-matrix composites based on their component material properties, but there is a poor understanding of the correlation of these models to the true physical basis for the models. The extent to which variations in fracture toughness can be attributed to factors such as crack deflection, crack-tip bridging, crack-front bowing, and interfacial adhesion, is an important area for new research. The objective of the present work has been to characterize the role of some of these factors by making dynamic observations of a propagating crack in a particle filled brittle matrix composite. High speed photography has been used to obtain photoelastic images of the state of stress at the leading edge of dynamic cracks as they intersect and pass disperse spherical particles in a birefringent polyester matrix. In order to further characterize the nature of the crack tip in the area of embedded spherical particles, cracks were also induced to arrest in close proximity to spherical particles in composite materials of the same type as used in the dynamic experiments.

Experiments were performed using brittle polyester matrix materials with embedded disperse spherical particles. The particles were of three types including steel, glass, and rubber. Three series of experiments were performed. In the first series of experiments the physical characteristics of a polyester matrix material were evaluated including tensile strength, elastic modulus and birefringent properties. The second series of experiments utilized a Cranz-Schardin camera, and a circular polarizer to study the state of stress at the tip of dynamic cracks during progression of the cracks past particles in Modified Compact Tensile (MCT) test specimens. The third series of experiments was performed using the same component materials as the MCT experiments, in the form of single edge notch (SEN) specimens. In these experiments cracks were induced to arrest in close proximity to the spherical particles.

Macrographic analysis of the fracture surfaces of the dynamic MCT samples, and observation of the arrested crack fronts in the SEN samples were then used to determine the path and shape of the leading edge of the dynamic crack. These crack front profiles were then directly correlated to the stress intensity and velocity profiles obtained in the dynamic photoelastic studies.

ACKNOWLEDGEMENT

TABLE OF CONTENTS

LIST OF TABLES

LIST OF FIGURES

CHAPTER I

INTRODUCTION

The characterization of crack-particle interactions, and the study of the effect that crack-particle interactions have on a material's fracture toughness, are important considerations in many composite material systems. Examples of composite materials with properties that have been enhanced by the addition of particles include brittle ceramics with improved fracture toughness from embedded ductile particles, and polymers toughened by the addition of rubber particles. The macroscopic properties of each of these particle-reinforced composites are dramatically influenced by the micromechanical deformations that occur in the area of the embedded particles.

The ability of two or more constituents to be effective as a composite depends on many factors including particle/matrix volume fraction, particle size, particle/matrix elastic modulus mismatch, matrix-particle adhesion, residual stresses, and also depends on the matrix and particle component properties, such as yield strength, plasticity/ductility and fracture toughness [1,2]. The interdependence and overall effect that each of these factors has on the toughness of a composite material is highly complex.

A considerable body of work exists that studies the behavior of particle-matrix composites. Many of these works are directed towards establishing a fundamental understanding of composite material behavior based on the mechanics of crack propagation in the area of a particle. These include works on crack tip bridging [3-6], crack front bowing [7,8], crack deflection [9-11], and the effects from particle matrix interfacial adhesion [12-13]. The experimental research presented in this paper builds on these fundamental concepts of fracture mechanics of particle filled composites. Also, since only a limited number of previous works

have studied crack-particle interactions under dynamic conditions [14-16], the present work expands the knowledge of the physics of interactions of a dynamic crack with embedded particles.

By making both static and dynamic observations of cracks near disperse particles in polyester matrix materials it becomes possible to make a careful analysis of several of the factors that influence crack propagation in particle reinforced composites. These include observations of the variation in the dynamic stress intensity factor near particles with elastic modulus much higher than, and also with elastic modulus lower than, the modulus of the polyester matrix materials. In addition the dynamic effects from crack tip bowing and partial crack tip bridging are observed as well.

CHAPTER II

REVIEW OF PREVIOUS WORK

2.1   Intrinsic Material Fracture Toughness, and the Crack Tip Process Zone

In 1920 Griffith described a material as having an intrinsic cohesive surface energy. He hypothesized that during fracture, the energy to cause incremental increase in the area of a crack (extension of the crack), derives from the increment in internal strain energy of the system, plus the incremental work from external forces, particularly when the process zone is small compared to all dimensions of the crack and the specimen

Since that time many works have come to distinguish the fracture toughness of materials as being provided by crack near-tip mechanisms, and in the limiting case of linear elastic fracture mechanics these mechanisms reduce to a material fracture toughness which can be described by a material constant. Depending on the mechanics of crack propagation in the near-tip process zones, the literature might refer to the process as occurring within the small-scale limits of Griffith's model. As these models of material behavior evolved to include cases of complex crack tip behavior, such as when there is plastic deformation near the crack tip, the crack-tip process zone came to be modeled as having a correction for this near-tip plastic behavior and the crack tip process zone was referred to as a Dugdale Zone. More recent representations of materials with complex behavior, such as those with microcracking, or transformation toughening, have been modeled by adding a correction to the near-tip process, and this category of models with near-tip corrections has been referred to as describing a cohesive crack tip zone.

In the case of models of crack propagation in reinforced composite materials, such as with reinforcements bridging the crack tip, the mechanics of fracture at the crack tip are sometimes

3

distinguished from the cohesive zone models as having a near-tip component of matrix material toughness, added to a distinct material toughness component from the reinforcements. The combined model from these two processes might be described as a "small-scale-bridging" model.

The following review of the literature describes the origin of these models with particular emphasis on the bridging models. The review is then concluded with a presentation of recent work that investigates processes in the near-tip zone including crack deflection, crack bowing, crack tip trapping and crack tip bridging.

2.2   Irwin's Energy Balance and Energy Release Rate/Stress Intensity Factor

Modern methods for analysis of crack tip stresses originated in 1920 with Griffith's [17] concept of energy balance, which was later refined by Irwin's [18] addition of an incremental measure of plastic work per unit of crack surface created. An outcome of these works was the concept of stress intensity at the crack tip and an intrinsic fracture toughness of a material.

Irwin and others developed closed-form solutions for the stresses in the area of a crack tip. These solutions for the state of stress near the crack tip in linear elastic materials describe the stresses as varying with the inverse of the distance from the crack tip ($1/\sqrt{r}$), and are asymptotic to the crack tip at radius equal to zero (stress field $\sigma_{ij} = k/\sqrt{r} \ f_{ij}(\theta) + $ other terms) [1]. The asymptotic region of stress at the crack tip is said to be the singular zone and is depicted below in figure 1. In this region the proportionality constant K, the stress intensity factor, defines the state of stress.

4

In 1961 Irwin [19] proposed that in the case of real materials with non-infinite stresses at the crack tip, the non-infinite stresses can be accommodated by defining a plastic zone at the tip of the crack. This "correction" by Irwin assigned an effective crack length which is the sum of the actual crack size and a plastic zone, represented by an "effective" stress intensity factor $K_{eff} = C\,(a_{eff})\,\sigma\,\sqrt{\pi}\,a_{eff}$, where a_{eff} is a geometry correction factor.
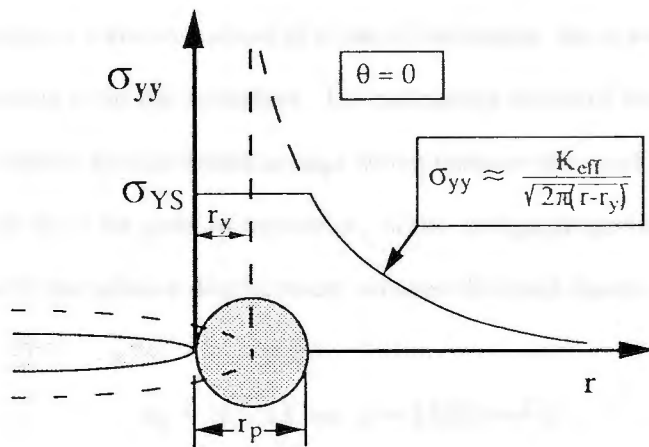
Figure 1 The crack tip stress field with Irwin's plastic zone correction [reproduced from 1 page 87]

The Irwin plastic zone correction.

2.3   Dugdale's and Barenblatt's Strip Yield Model

In 1959 Barenblatt [20,21] proposed the first of what later came to be known as "cohesive zone" models. In Barenblatt's model the complex elastic-plastic crack tip behavior of brittle heterogeneous materials is represented as the superposition of two simpler models. Barenblatt described a zone at the crack tip with finite stresses that are modeled in a plastic zone of length ρ. In this zone the normally singular elastic crack under remote tension is superimposed over an elastic crack having closure stresses at the tip. In this way the stress singularity of the otherwise perfectly elastic crack tip is summed with, and made real by, the closure stress acting over the same region of the crack tip. Shortly after Barenblatt's work, Dugdale [22] applied a similar method of superposition (the strip yield model) to the analysis of fracture of more ductile materials.

5

2.4   Rose's Distributed Spring Model

In 1987 L.R.F. Rose [23] proposed a distributed springs model for crack front bridging that was consistent with earlier work by Marshall, Cox and Evans in 1985 [24] and Budiansky, Hutchinson and Evans in 1986 [25]. In Rose's model a crack front is considered that has progressed a distance ahead of a line of inclusions, but is held back by unbroken ligaments stemming from the inclusions. The restraining action of these unbroken ligaments is represented by distributed springs acting between the crack faces. The springs are linearly elastic up to the point of rupture, σ_y of the springs proportional to the spring stretch δ (which is equal to the relative displacement between the crack faces),

$$\sigma_y = \tfrac{1}{2} E'k\delta \;\; or, \;\; \sigma = Ek\delta/(1\text{-}v^2)$$

$$k = \text{spring constant} \quad \delta = \text{crack displacement} \quad E' \equiv E/(1\text{-}v^2)$$

Rose developed a solution for the stress intensity factor K, and the maximum stretch of his idealized springs δ_{max}, as follows:

$$K = \{\sigma\,(\pi\,a)^{1/2}\}F(kl;c/a)$$

$$\text{and }\; \delta_{max} = \{(4\sigma/E')(a^2 - c^2)^{1/2}\}V(kl;c/a)$$

where the terms in brackets refer to the values of K and δ_{max} for a crack without reinforcements. The terms F and V are normalization functions that are derived by applying Bilby's and Eshelby's analysis [26,27] of the perturbation of a stress field in the presence of a crack. Rose's solution to the perturbed crack with springs/ligaments is a dislocation density along the length of the crack that satisfies the Bilby/Eshelby analysis, and also has an inverse square root singularity at the crack tips. As part of Rose's analysis, he derived solutions of the

6

crack dislocation density that were dependent on the nondimensional crack length parameter of c/a and nondimensionalized spring-crack parameter kl. Rose applied this concept of bridging ligaments to a range of cracks, from the case of small scale bridging (c/a → 1), up to reinforcement from a fully bridged crack (c/a = 0). He developed models which employed hard springs (kl >> 1), and soft springs (kl << 1), as well as linear and nonlinear springs, and used interpolating functions and numerical solutions for springs of intermediate stiffness.

2.5   Bridged versus cohesive crack tip models

Barenblatt's and Dugdale's models for the non-linear processes at the crack tip have come to be known as cohesive-zone models. The cohesive zone is comprised of a region with tractions between the faces of the crack, acting in opposition to the applied load. This non-linear cohesive zone, would normally be a singularity-dominated region at the crack tip of a perfectly elastic material, with a stress intensity K_σ resulting from the remotely applied stress σ. But in the case of the cohesive model the K_σ singularity is balanced by the closing tractions acting in the plastic region with a closure stress intensity of $K_{closure}$. The net stress intensity factor at the crack tip $K_\sigma + K_{closure}$ is a non-singular value, and the tractions give a continuous normal stress in the non-linear region thereby modeling the elastic-plastic behavior near the crack tip. These tractions, such as Dugdale's yielding of metals, govern the opening displacement in the zone, and also define the separation of the crack faces at the wake of the zone.

Rose's model is characteristic of a second class of models of crack tip behavior (distinguished from the cohesive models of Dugdale and Barenblatt) known as bridged crack models. While the bridged crack models, like the cohesive models, have tractions between the crack faces, in the bridged crack models the non-linear separation processes allow for a singularity-dominated region at the crack tip. As a result, the bridged crack models can be used to represent non-

7

linear regions with more than one physical phenomena such as fracture events with distinct tip and wake phenomena. For example, a bridged crack model of a fiber-matrix or particle-matrix composite has brittle fracture of the matrix (a singularity in the non-linear region), in combination with tractions from crack bridging phenomena such as fiber or particle pullout processes that also occur in the non-linear region, but which might be behind the brittle fracture event.
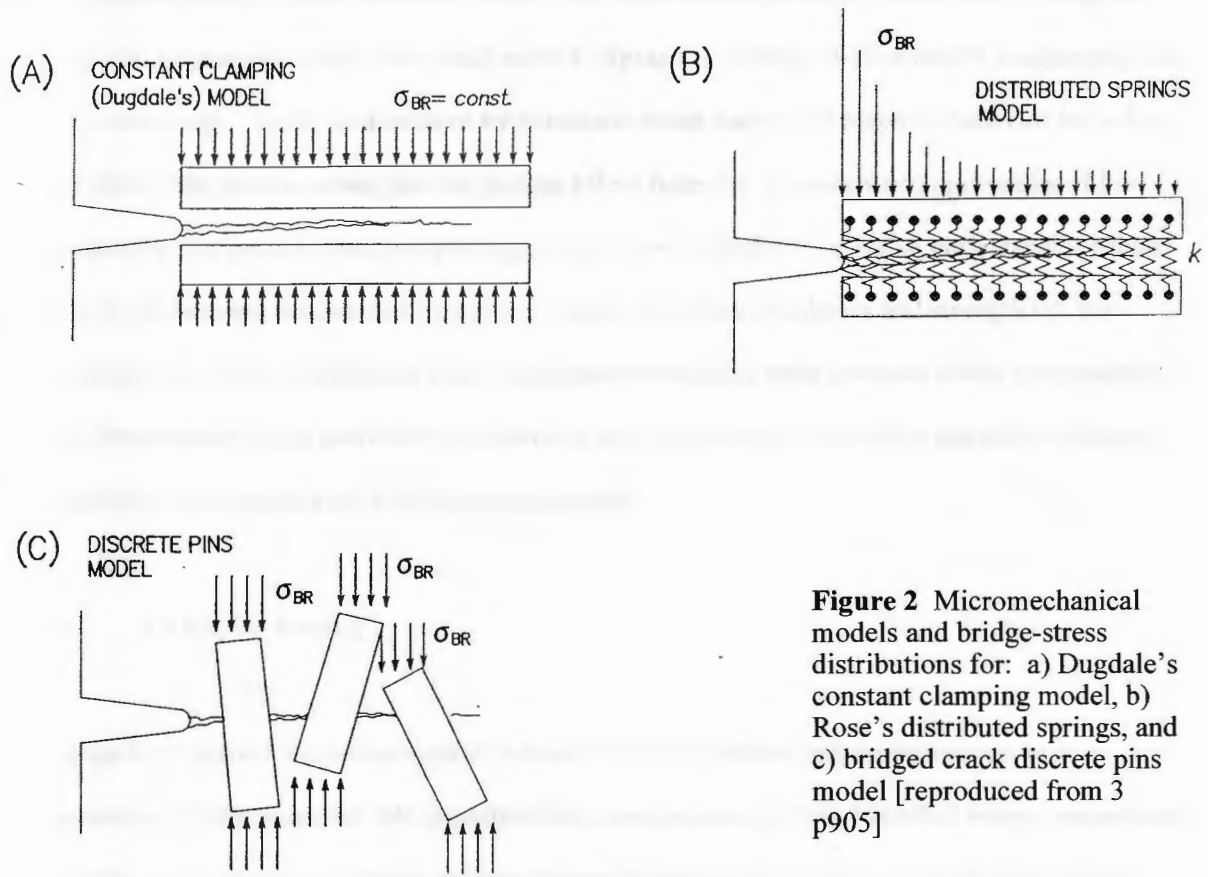
Figure 2 Micromechanical models and bridge-stress distributions for: a) Dugdale's constant clamping model, b) Rose's distributed springs, and c) bridged crack discrete pins model [reproduced from 3 p905]

Small-scale limiting cases of both the cohesive and bridged crack models are when the crack tip zone is small compared to all dimensions of the crack and specimen. And in both cases the increment in toughness from the crack tip process zone is a material constant. Linear Elastic

Fracture Mechanics apply in this small-scale limit and a critical value for the Stress Intensity Factor exists.

2.6   Recent work relating to particle reinforced composites

Since 1970, studies of means for improving the fracture toughness of particle reinforced brittle composite materials have focussed on two main near-tip toughening mechanisms. These are crack deflection, and crack face small-scale bridging (excluding transformation toughening and microcracking). These studies have emphasized certain aspects of material behavior including the size of the process-zone, the toughening effect from the microstructural geometry of the composite (i.e. particle size, morphology, orientation, interfacial adhesion etc.) and the effects due to the inherent mechanical properties (elastic modulus, toughness and strength) of the constituents. The contributions from these parameters have been assessed both experimentally and theoretically, with particular emphasis on the size of the process-zone and the toughening contribution by small scale bridging mechanisms.

2.7   Crack tip bowing

Lange [28] studied the interactions of a crack front with second phase dispersions in a composite, brittle material. He hypothesized, based on the Griffith Model of energy absorption, that the major energy-absorbing process during fracture is the production of surface energy. Lange speculated (based on experimental observations) that fracture energy increases when inhomogeneities in a brittle material act as obstacles to progression of a crack front. Increased fracture toughness results from "crack bowing" when the crack front increases its length as it is simultaneously pinned by two or more inhomogeneities. Lange's model supposes that the crack front bows out between the second-phase dispersion while still remaining pinned at all the

9

positions where it encounters the dispersion. During crack propagation, both new fracture surface is formed and the length of the crack front is increased due to its change in shape between the pinning positions. Using this model a functional relation between the fracture energy and the dispersion spacing is derived for the case of a Griffith crack under an applied tensile stress. Lange states that "...the increment of energy absorbed (ΔU) for an increment of crack extension (ΔC) can be divided into two parts, i.e. one part (ΔU_S) associated with the energy to form new surface area and one part (ΔU_L) associated with the energy to form the increased length of the crack front."

Evans [29] concluded that toughening cannot only be due to particle spacing, and added to Lange's model for crack front bowing by also relating toughening to the inclusion-size-to-spacing ratio, rather than just the spacing.

Green et.al. [30,31] studied crack shape changes in the vicinity of un-bonded spherical nickel inclusions in a glass matrix. Green postulated that observed increases in fracture energy resulted from crack tip blunting although increased toughness was less than predicted by theory.

2.8   Crack plane deflections

In 1980 Cotterel and Rice [32] solved for the increased driving force necessary to propagate a crack subjected to a local planar tilting misalignment (crack deflection). In their work the tilted stress intensity factors K^t_I and K^t_{II} and K^t_{III} are solved for and stress intensity is plotted as a function of angle of inclination of the crack.

Faber and Evans [9,10] by a geometrical analysis extended Cotterel's and Rice's planar solution to three dimensions (crack deflection including tilting and twisting). They deduced that tilted

10

cracks have mode I opening, and II sliding components, while twisted cracks have mode I and mode III tearing components. Toughening, and crack advance are presumed governed by the strain energy release rate G from the segment of the mis-aligned crack. The effects from aspect ratio of the particles, and particle spacing, were studied for both rods, discs and spheres. This geometrical analysis predicts that tilt is non-contributing to fracture toughening, except in the case of discs, where tilt provides a small benefit. In all cases crack deflection by twisting is the predominant toughening mechanism (refuted later by Pezzotti 1993 [11]), and rods of high aspect ratio are the most effective for deflecting cracks with increased toughness as high as 4 orders of magnitude for rods with aspect ratio of 12 or higher.

Pezzotti [11] performed toughness experiments, and carefully analyzed particle spacing, and crack and matrix morphology of the fracture surfaces using image analysis techniques. The results of these experiments were used as aids to model toughness enhancements from various crack front deflection configurations. Near-neighbor spacing measured in Pezzotti's experiments differ from spacings deduced by Faber/Evans [9,10] by geometric techniques, and account for overestimates of 3 or more orders of magnitude toughness enhancement by the Faber/Evans model. "It is shown that the actual contribution of crack-deflection as a toughening mechanism itself is generally small ($\leq$40% in terms of K_{Ic} increase) even when maximum deflection can be achieved, and it is limited by reasons related to the microstructural arrangement of the second phase inside the matrix." [11 p1838].

2.9   Crack pinning

As noted above, in 1970 Lange speculated (based on experimental observations) that fracture energy increases when inhomogeneities in a brittle material act as obstacles to progression of a

crack front. Increased fracture toughness results from "crack bowing" when the crack front increases its length as it is simultaneously pinned by two or more inhomogeneities.

In 1985 Rice [33] developed a three dimensional weighted function theory to study stress intensity factors along a nonlinear crack front. The numerical methods allowed first-order elastic field variations due to varying crack front geometry to be analyzed.

Rose [34] proposed that a two-phase stress intensity factor can be used to model the restraining effect of inclusions. In the case of a bowed crack front between inclusions, Rose characterizes unbroken ligaments stemming from the inclusion and behind the furthest extent of the crack front as "stretched" ligaments which toughen the matrix. The two-phase parameter which accounts for crack front bowing and "crack bridging" is dependent on inclusion size, spacing and volume fraction and describes a property of the two-phase composite which is not necessarily related to the properties of the separate phases. Rose's parameter correctly characterizes the volume fraction dependence of the fracture toughening seen in Lange's experiments.

Evans, Budiansky and Amazigo [4] performed theoretical analysis of elastic-perfectly plastic particles bridging crack faces, spaced to simulate a brittle ceramic bridged by ductile metal particles, and compared their analysis to experimental results. They employed Budiansky's and Rose's distributed spring model for the partially pinned crack. Their model utilizes an elastic spring constant which they derive based on a randomly distributed concentration of "smooth punch" bridging elements. They studied the toughening effects of particle spacing (volume concentration), and from ductility of the bridging elements. In their model they conclude that "Confrontation of experimental data on metal-reinforced ceramics with the predictions of the present theory seems to imply suspiciously high particle strengths. If such high strengths are

not confirmed, toughening mechanisms in addition to crack bridging may be operative in particulate-reinforced ceramics."[4 p181]

Rice and Gao [8] used Rice's technique to study variations in elastic fields as a crack front penetrates (is trapped by) an array of obstacles. They assumed that progressive states of equilibrium occurred as the applied load increased and the crack front moved forward to achieve a geometry where the stress intensity factor is matched to the local fracture toughness. Their first-order model extends only to cases of particle toughness close to matrix toughness and also only in cases of crack bowing aspect ratios up to approximately 1.2

Fares [35] used Boundary Element Methods to discretize crack growth profiles. The BEM method can be applied to wider bounds of particle/matrix toughness ratios than Rice's, and also, the BEM method models observed crack behavior more closely including cases when the crack fronts circumvent obstacles leaving bridged particles behind the crack front.

Bower and Ortiz [36] extend Rice's first-order perturbation analysis to include large perturbations by beginning with a known initial geometry (such as a circular or half-plane crack) and using a succession of perturbations to calculate stress intensity factors. As examples of the method they present solutions to the problems of a semi-infinite crack trapped by a periodic array of tough particles, and unstable growth of a semi-infinite crack through material of decreasing toughness. A difficulty associated with the method is the presence of singularities in the integral calculations. The singularities are regularized using the known behavior of cracks (generally known only for planar cracks). Continuity is preserved by using weighted interpolation in the area of the singularities.

13

Bower and Ortiz [6] went on to apply perturbation analysis of crack propagation to include particles which remain intact after a crack front has bowed and then coalesced, after propagating past the particle. This is the case of crack bridging. As the crack faces separate the particles ultimately fail either by fracture or pullout depending on the strength of the particle matrix bond. This model is for the case of elastic modulus of the particles near the modulus of the matrix. In the case of particles with good adhesion and higher elastic modulus, cracks are deflected around the particles. In the case of particles with toughness less than three times the matrix toughness, the particles are penetrated and fractured by the crack. The most effective mechanisms for toughening are crack trapping (bowing) and bridging which can improve toughness by a factor of five or more as compared to crack deflection (high modulus particles) and crack tip microcracking which result in 20-30 percent improvements.

Bower and Ortiz [7] extend the application of the incremental perturbation method to the case of an initially straight crack propagating through a sinusoidal residual stress field. The problem can be depicted qualitatively as distributed regions of residual tension and compression. The regions are self equilibriating (averaging) in a global sense. However transient toughening occurs as a crack front is trapped by compressive zones and becomes bowed as it accelerates through intermediate tensile regions. As the bowed crack progresses it alternately encounters regions of higher and lower fracture toughness around a mean value. In the case of high residual compressive stresses "pinned" regions (crack bridging) may be left in the wake of the crack. But, for practical values of residual stress the enhancement of toughness is not significant.

Mower and Argon [14] studied the process of crack trapping by high toughness inclusions that had elastic modulus near the matrix modulus. The result is crack bridging by the tough particles. The effects of particle size, spacing, adhesion and residual stresses on the crack front

14

behavior and toughness were observed. Bowed crack front shapes were seen to match Bower's and Ortiz's predictions very well.

While working with particle reinforced ceramics Pezzotti [11] differentiated between toughening achieved by microfracture mechanisms at the crack tip, from those in the wake zone following behind the crack tip. His small scale bridging model describes these two toughening effects that can give rise to R-curve behavior because of the potentially cumulative nature of the wake zone effects. In 1996 Pizzotti et al. [3] studied the possible existence of an intrinsic fracture toughness value in ceramic composites. They described both the Dugdale and the distributed spring models as involving shielding-stress distribution functions which are continuous over the entire range of crack length. They contrasted a continuous stress distribution for fiber-reinforced materials, to the observed R-curve ("pop-in") behavior in particle reinforced ceramics experiments, and concluded that a discrete stress function is more physically realistic when the inter-particle distance is of the same order of magnitude as the bridging zone length. When only one or few particles act as the bridges in the wake of the pop-in crack, Pezzotti et al. modeled the particles behavior as stiff nails held between the crack faces and locally exerting point forces that pin the crack faces. They performed FEM calculations assuming infinite strength of the interface, and with bridging particles that were considered to behave elastically. They generally found that, in the range of Young's modulus and strength reported for ceramic single-crystals, no more than one single particle could operate elastic bridging whatever the volume fraction, which was consistent with the particle morphology in their experiments.

2.10   Crack path selection

Erdogan et. al. [37] discuss crack propagation of an arbitrarily oriented crack near an inclusion
and the tendency of a crack to propagate towards or away from a perfectly bonded inclusion
depending on relative elastic properties. They use the "single-valuedness condition of
displacement" [37 p1009] and the superposition of the problems of 1) stress distribution near a
circular inclusion without the crack, and the problem of 2) stress disturbance of the normal and
tangential stresses resulting from the presence of a crack, to calculate stress-intensity factors.
Their result predicts that a crack will propagate toward an inclusion if the inclusion modulus is
less than the matrix and away if the inclusion has higher modulus.

Dekkers and Heikens [38] found that the mechanisms for craze formation near glass beads in a
matrix are fundamentally different for adhering and non-adhering beads. In the case of
excellent interfacial adhesion the crazes form near the pole of the beads in regions of maximum
dilatation and of maximum principal stress. With poor interfacial adhesion the crazes form
along the interface between pole and equator and originate at an angle θ of about 60°. In this
case de-wetting proceeds along the phase boundary in the direction of the equator, and because
of that a small cap-shaped cavity is formed which lies around the top of the sphere. As the
sharp edge of the cavity gradually approaches the equator, de-wetting becomes more difficult as
a consequence of the contraction of the matrix perpendicular to the applied tension. At a certain
angle θ de-wetting stops because it is energetically more favorable to start a craze at the edge of
the cavity.

Evans, Dalgleish, He and Hutchinson [39] studied the conditions required for a crack
propagating in an interface to kink out of the interface. The tendency to propagate in the
interface depends on the phase angle (ψ) of the mixed mode state of stress at an interface. Here

16

the mode mixity is defined as: $\psi = \tan^{-1}$ (K_{II} / K_I). Normally a crack growing in a homogeneous material tends towards a mode I path. They demonstrated that the choice of test specimen can govern the tendency of cracks to either remain at the interfaces or deviate away, based on the phase angle of loading. The sign and magnitude of ψ dictate whether cracks either propagate along the interface, or deviate into the adjoining material and extend parallel to the interface. They found that for a given combination of opening and shear loading at the tip of an interfacial crack, as characterized by the phase angle ψ, there is a critical ratio of interfacial and matrix toughness, R_I /R_m , which must not be exceeded if the crack is to remain in the interface. They showed that the measured interface fracture energy may be strongly influenced by the crack trajectory, as governed by ψ, due to crack shielding and plasticity effects.

Lefebvre, Gerard et al. [40] studied the influence of an elastomeric interface layer on the fracture properties of glass beads in an epoxy matrix. The critical stress intensity is seen to increase fracture toughness and is attributed to the promotion of shear yielding in a localized zone near the crack tip.

Lee, et al. [41] considered whether a driving force for a crack to grow along a remote interface can exceed the fracture energy of the interface, before the driving force for the primary crack approaching the interface exceeds the fracture energy for the matrix. They found that an interface may deflect primary cracks once it contains defects and there is enough driving force for its growth. However, this is true only when the interface debond crack does not kink out of the interface and when the primary crack stops with no further crack growth. They studied these behaviors by making static observations of the morphology of cracks which they had caused to arrest in Single-Edge-Notch specimen fracture experiments.

17

CHAPTER III

THEORETICAL ASPECTS OF BIREFRINGENCE AND STRESS STATE AT THE TIP OF A DYNAMIC CRACK

Particle-filled composites generally exhibit isotropic behavior. This is because the particles are uniformly distributed, and the physical behavior of the composite is symmetric in three dimensions. In some cases, such as injection-molded components where particle alignment might occur due to the molding process, particle filled composites can exhibit a higher degree of anisotropy. However, the experiments reported here study the behavior of symmetric particles embedded in a matrix.

In order to isolate the effects of interaction between a dynamic crack and a single embedded particle, experiments were performed on materials comprised of disperse spherical particles in a brittle matrix. By having spacing of approximately 5 diameters between particles and a total matrix thickness of approximately 4 diameters, the effects from particle interactions were minimized. In this way, observations were made of dynamic cracks propagating through an orthotropic medium, and of the dynamic crack encountering disperse embedded particles in the medium. Khanna [13], in dynamic photoelastic and strain gauge experimental work, calculated that the correction factor for dynamic stress intensity factor due to the effect of materials bridging the crack tip in an orthotropic medium is less than 2%. The experimental work presented in this paper utilizes photoelastic methods for orthotropic media in making determinations of stress intensity. The theoretical basis for determining the stress intensity factor and stress field around a dynamic crack in orthotropic materials is presented here.

Sanford's and Dally's [42] over-deterministic solution relating stress intensity factors at a crack tip to isochromatic fringes using Irwin's series representation of the stress field around constant speed cracks [43]

Irwin's series representation of the stress field around a constant speed crack expresses the stresses at the crack tip as a power series containing $r^{(n-1)/2}$ terms. The birefringent behavior of polyester matrix materials allows stresses to be observed as dynamic isochromatic fringes at the tip of a crack propagating at high velocity. Since the isochromatic fringes represent the contours of constant maximum in plane shear stresses τ_m in the field around the crack tip, observed fringe data can be coupled to Irwin's stress field equations to solve for the stress intensity factor K_I at the crack tip. Irwin's dynamic crack tip stress field equations are as follows:

$$\sigma_x = \frac{1 + \lambda_2^2}{4\lambda_1\lambda_2 - (1 + \lambda_2^2)^2}\{(1 + 2\lambda_1^2 - \lambda_2^2)\operatorname{Re} Z_1 - \frac{4\lambda_1\lambda_2}{1 + \lambda_2^2}\operatorname{Re} Z_2\} + \frac{1}{\lambda_1^2 - \lambda_2^2}\{(1 + 2\lambda_1^2 - \lambda_2^2)\operatorname{Re} Y_1 - (1 + \lambda_2^2)\operatorname{Re} Y_2)$$

$$\sigma_y = \frac{1 + \lambda_2^2}{4\lambda_1\lambda_2 - (1 + \lambda_2^2)^2}\{(1 + 2\lambda_1^2 - \lambda_2^2)\operatorname{Re} Z_1 - \frac{4\lambda_1\lambda_2}{1 + \lambda_2^2}\operatorname{Re} Z_2\} + \frac{1 + \lambda_2^2}{\lambda_1^2 - \lambda_2^2}(\operatorname{Re} Y_2 - \operatorname{Re} Y_1)$$

$$\tau_{xy} = \frac{2\lambda_1(1 + \lambda_2^2)}{4\lambda_1\lambda_2 - (1 + \lambda_2^2)^2}\{\operatorname{Im} Z_2 - \operatorname{Im} Z_1\} + \frac{1}{(\lambda_1^2 - \lambda_2^2)}\{\frac{(1 + \lambda_2^2)^2}{2\lambda_2}\operatorname{Im} Y_2 - 2\lambda_1\operatorname{Im} Y_1\}$$

Where:

$$Z_j = Z(z_j) = \sum_{n=0}^{n=N} C_n z_j^{n-1/2} \ , \ j = 1,2,3$$

$$Y_j = Y(y_j) = \sum_{m=0}^{m=M} D_m z_j^{m} \ , \ j = 1,2,3$$

with: $z_j = x + i\lambda_j \ y, \ j = 1, 2, 3$

$\lambda_j = 1 - (\mathring{a} / c_j)^2, \ j = 1, 2, 3$

and where: $\mathring{a}$ is the crack velocity

c_1 is the plate wave speed

c_2 is the shear wave speed

x, y are coordinates with origin at the crack tip

Using the first three terms in each of the series Z and Y, then Z_1, Z_2, and Y_1, Y_2 can be expressed as:

$$Z_1 = C_0 z_1^{-1/2} + C_1 z_1^{1/2} + C_2 z_1^{3/2}$$

$$Z_2 = C_0 z_2^{-1/2} + C_1 z_2^{1/2} + C_2 z_2^{3/2}$$

$$Y_1 = D_0 z_1^{-1/2} + D_1 z_1^{1/2} + D_2 z_1^{3/2}$$

$$Y_2 = D_0 z_2^{-1/2} + D_1 z_2^{1/2} + D_2 z_2^{3/2}$$

Here $C_0 \sqrt{2\pi}$ is K_I, the stress intensity factor, and $2 D_0$ is the remote stress σ_x

Remembering that the maximum in-plane shear stress τ_m is related to the Cartesian components of stress (thus to the isochromatic fringes) by:

20

$$(2\tau_m)^2 = (N f_\sigma/h)^2 = (\sigma_X + \sigma_Y)^2 + (2\tau_{XY})^2$$

Substitution of Irwin's dynamic stress field equations into the stress optic relationship gives expressions for $(\sigma_X - \sigma_Y)$ and (τ_{XY}) in terms of the series constants and the coordinates of the point x , y in the region of the crack tip, and relates them to the fringe order around the crack tip. This is a system of non-linear equations to be solved for the unknown coefficients C_n and D_m . The over-deterministic method of Sanford and Dally, which is described below, can be used to solve for the unknowns.

Sanford's and Dally's method, as it applies to static stresses at a crack tip is as follows:

The local stresses in the neighborhood of crack tip are:

$$\sigma_x = \frac{1}{\sqrt{(2\pi r)}}[K_I \cos\tfrac{\theta}{2}(1 - \sin\frac{\theta}{2}\sin\frac{3\theta}{2}) - K_{II} \sin\tfrac{\theta}{2}(2 + \cos\tfrac{\theta}{2}\cos\tfrac{3\theta}{2})] - \sigma_{0x}$$

$$\sigma_y = \frac{1}{\sqrt{(2\pi r)}}[K_I \cos\tfrac{\theta}{2}(1 + \sin\frac{\theta}{2}\sin\frac{3\theta}{2}) - K_{II} \sin\tfrac{\theta}{2}\cos\tfrac{\theta}{2}\cos\tfrac{3\theta}{2})]$$

$$\tau_{xy} = \frac{1}{\sqrt{(2\pi r)}}[K_I \sin\frac{\theta}{2}\cos\tfrac{\theta}{2}\cos\frac{3\theta}{2} + K_{II} \cos\tfrac{\theta}{2}(1 - \sin\tfrac{\theta}{2}\sin\tfrac{3\theta}{2})]$$

with r and θ being polar coordinates (r/a << 1), and with the origin at the crack tip. The term σ_{0x} is a correction term for specimen geometry (from Irwin, Proc. of SESA 16, 93-96 1958)

The maximum in-plane shear stress τ_m is related to the Cartesian components of stress (and to the isochromatic fringes) by:

$$(2\tau_m)^2 = (\sigma_x - \sigma_y)^2 + (2\tau_{xy})^2 = (N\,f_\sigma/h)^2$$

Combining these equations gives the relation for the isochromatic fringe pattern in the area of the crack tip:

$$(Nf_\sigma / h)^2 = \frac{1}{(2\pi r)}[(K_I \sin\theta + K_{II}\cos\theta)^2 + (K_{II}\sin\theta)^2] +$$

$$\frac{2\sigma_{0x}}{\sqrt{(2\pi r)}}\sin\frac{\theta}{2}[K_I \sin\theta(1+2\cos\theta) + K_{II}(1+2\cos^2\theta+\cos\theta)] + \sigma_{ox}^2$$

Sanford and Dally went on to solve for the unknowns ($\mathbf{K_I}$, $\mathbf{K_{II}}$ and σ_{0x}) of this nonlinear equation by the Newton-Raphson method.

define:

$$g_k(K_I, K_{II}, \sigma_{0x}) = 0 = \frac{1}{(2\pi r)}[(K_I \sin\theta + 2K_{II}\cos\theta)^2 + (K_{II}\sin\theta)^2] +$$

$$\frac{2\sigma_{0x}}{\sqrt{2\pi r}}\sin\frac{\theta}{2}[K_I \sin\theta(1+2\cos\theta) + K_{II}(1+2\cos^2\theta+\cos\theta)] +$$

$$\sigma_{0x}^2 - (Nf_\sigma / h)^2$$

with k being the number of undefined data points on fringes of the stress field in question.

Substituting estimates for the unknowns into this equation results in an error, since, using values that are only an estimate g_k would then not be equal to zero. But, a Taylor Series expansion of g_k leads to the equation:

22

$$(\partial g_k / \partial K_I)_i \Delta K_I + (\partial g_k / \partial K_{II})_i \Delta K_{II} + (\partial g_k / \partial \sigma_{0x})_i \Delta \sigma_{ox} = -(g_k)_i$$

with i being the i_{th} iteration.

Given k data points from a fringe pattern at a crack tip, and k equations with unknowns ΔK_I, ΔK_{II} and $\Delta \sigma_{ox}$, then a set of over-determined linear equations of the form given below is the result.

$$
\begin{bmatrix} g_1 \\ g_2 \\ . \\ . \\ . \\ g_k \end{bmatrix}_i =
\begin{bmatrix}
\dfrac{\partial g_1}{\partial K_I} & \dfrac{\partial g_1}{\partial K_{II}} & \dfrac{\partial g_1}{\partial \sigma_{0x}} \\
\dfrac{\partial g_2}{\partial K_I} & \dfrac{\partial g_2}{\partial K_{II}} & \dfrac{\partial g_2}{\partial \sigma_{0x}} \\
. & . & . \\
. & . & . \\
. & . & . \\
\dfrac{\partial g_k}{\partial K_I} & \dfrac{\partial g_k}{\partial K_{II}} & \dfrac{\partial g_k}{\partial \sigma_{0x}}
\end{bmatrix}_i
\begin{bmatrix} \Delta K_I \\ \Delta K_{II} \\ \Delta \sigma_{0x} \end{bmatrix}_i
$$

which in matrix form can be written as: $\quad$ **[g] = [a] [Δk]**

The least squares solution for [Δk] can be found from:

$$[\Delta k] \; = \; [c]^{-1} \; [d]$$

where: $\quad [d] \; = \; [a]^T \; [g]$

$\quad\quad\quad\quad [c] \; = \; [a]^T \; [a]$

and where: $\quad [c]^{-1}$ is the inverse of [c] and

$\quad\quad\quad\quad\quad [a]^T$ is the transpose of [a]

23

Then, by iteration, the solution for $[\Delta k]$ can be used to correct the previous estimates for K_I, K_{II} and σ_{ox} by:

$$(K_I)_{i+1} = (K_I)_i + \Delta K_I$$

$$(K_{II})_{i+1} = (K_{II})_i + \Delta K_{II}$$

$$(\sigma_{ox})_{i+1} = (\sigma_{ox})_i + \Delta\sigma_{ox}$$

This is repeated for several iterations until the solutions converge.

In the case of the dynamic stress field equations above, and using the over-deterministic method of Sanford and Dally, g_k (the k_{th} term of g) is first represented in the form:

$$g_k (C_0, C_1, \ldots D_0, D_1, \ldots) = 0 = (\sigma_x - \sigma_y)^2 + (2\tau_{xy})^2 - (N f_\sigma/h)^2$$

Having already substituted the series Z and Y into Irwin's dynamic stress field equations to give expressions for $(\sigma_x - \sigma_y)$ and (τ_{xy}) in terms of the series constants and in terms of the coordinates of the k_{th} point x, y in the region of the crack tip, we now have a system of non-linear equations to be solved for the unknown coefficients C_m and D_m. Sanford's and Dally's iterative least-squares solution to the over-determined Taylor-series expansion of the function g can now be used to solve for the dynamic stress intensity factors from the experimental fringe patterns.

CHAPTER IV

EXPERIMENTAL PROCEDURE

4.1   Purpose

The purpose of this experimental research has been to study the effects of embedded spherical particles on the propagation of dynamic cracks. Previous works by Theocaris and Milos [15], and Theocaris and Demakos [16] have studied dynamic particle-crack interactions using the method of caustics. Works by Mower and Argon have simulated dynamic fracture by load displacement analysis of slow stable crack propagation at low -60°C temperatures [14]. An alternate method for studying dynamic crack-particle interactions is presented here. This method employs the birefringence of brittle polyester materials to allow isochromatic images of the state of stress at the tip of dynamic cracks to be captured photographically. Also, static images of the shape of crack fronts arrested near embedded particles were used to learn more about the modes of crack propagation near particles. The experimental methods have been as follows:

4.2   Component materials properties of spherical particles

Tests were performed using three alternate spherical particle materials including low-leaded glass, low-carbon steel (manufactured by C&S Engineering Inc.), and Buna-N rubber spheres (manufactured by Precision Plastic Ball Company).

Table 1.   Particle Material Properties

Material	Tensile Strength (MPa)	Durometer (Shore A)	E Modulus (MPa)	Ultimate Elongation (%)
Buna-N Rubber	19	70	8.5	585
Low-Carbon Steel	400	N/A	200	25
Leaded Glass	1,200 (compressive)	N/A	62	1

4.3   Matrix Material Properties

A catalyzed polyester casting resin was used to form the matrix component of the composite specimens.   The resin was polyester type 458-C, manufactured by Polychem Corporation in Cranston, RI. In preparation for the dynamic photoelastic experiments, static experiments were performed to determine the material's elastic modulus, tensile strength, photoelastic fringe coefficient and critical stress intensity. The 458-C Polyester material properties were determined experimentally as follows:

4.4   Experimental Determination of Tensile and Elastic Properties

Two tensile test specimens were prepared and tensile tests were performed to determine the 458-C polyester tensile strength and elastic modulus. The tests were performed in an Instron tensile test machine with the following results:

Table 2.   Matrix Material Properties

Tensile Strength	55 MPa
Elastic modulus, E	4.2 MPa

4.5   Coefficients of thermal expansion

The thermal expansion coefficients of each of the component materials are as follows:

Table 3. Coefficients of Thermal Expansion

Material	α Thermal Expansion Coefficient (mm/mm/°C)
PolyChem 458-C Polyester	6×10^{-5}
Buna-N Rubber	19×10^{-5}
Low-Carbon Steel	11×10^{-6}
Borosilicate Glass	12×10^{-7}

4.6   Experimental Determination of Fringe Coefficient

Two approximately 1/2 inch thick samples with 2.87 inch diameter were incrementally loaded in a compression load test fixture, with polarized wave plates in place to determine fringe order as a function of load. The fringe constant, $f_\sigma = (8/\pi D)\ P/N$ where D is the specimen diameter, P is the compressive load and, N is the fringe order. A plot of the results from one of the samples, and the average material fringe value from the two experiments are shown below.

Figure 3. f_σ Calibration plot - 458c polyester
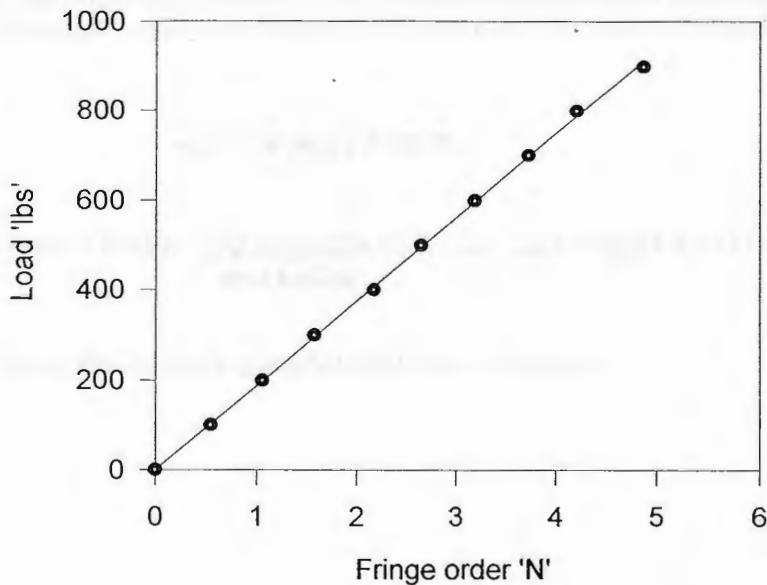
Table 4.   458-C Polyester Fringe Coefficient

Material fringe value, f_σ	MPa-m / fringe
PolyChem 458-C Polyester	.0304

4.7   Experimental Determination of Critical Stress Intensity Factor K_{IC}

Single Edge Notched Tensile (SENT) specimens comprised of cast and machined 456-C

Polyester panels with the dimensions shown in Figure 4 were loaded in a tensile test machine

until failure, with load increasing at 4 pounds per second.
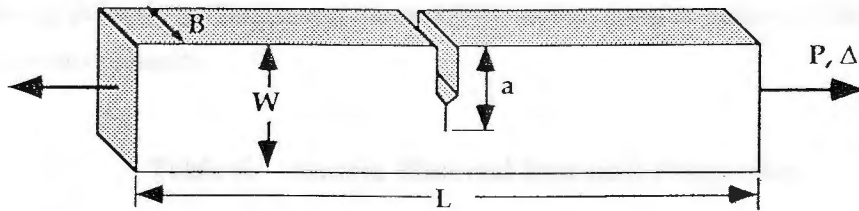
Figure 4. Single edge notched tension (SENT) panel.

reference: ASTM E 399, "Standard Test Method for Plane-Strain Fracture Toughness of Metallic Materials", American Society for Testing and Materials, Philadelphia, 1983

$$K_{IC} = f(^a/_W) \, P / (B\sqrt{W})$$

where: $f(^a/_W) = \dfrac{\sqrt{2}\,\tan(\pi a/2w)}{\cos(\pi a/2w)} \left[0.752 + 2.02\,(^a/_W) + 0.37\,(1 - \sin(^{\pi a}/_{2W})^3 \right]$

Results for the three samples tested were as follows:

Table 5.   458-C Polyester Matrix Critical Stress Intensity K_{IC}

	1	2	3
Thickness (inches)	0.50	0.50	0.53
Load at fracture (pounds)	238	226	208
K_{IC} (psi√in, MPa√m)	545 / 0.59	527 / 0.57	498 / 0.54

With average: K_{IC} **523 psi√in   0.57 MPa√m**

4.8   Dynamic Properties of Polyester Epoxy

The dynamic properties of polyester resin MR17090 by Aristech Chemical Corp., USA were determined previously by Shukla and Khanna [13], and are used as values for the 458-C polyester in this research.

Table 6.   Matrix Material Dynamic Properties

Dilatation wave velocity, c_1	2,200 m/s
Shear wave velocity, c_2	1,200 m/s
c_1 / c_2	1.83
Von Schmidt angle, θ	34.5°
$1/\sin\theta = (c_1 / c_2)$	1.76
Average Value of c_1 / c_2	1.79
Shear modulus, μ	1.70 GPa
Poisson's ratio, ν	0.37
Elastic modulus, E	4.65 GPa

4.9   Fabrication of composite samples with disperse spherical particles

After the matrix and particle component properties were determined, the materials were then used to fabricate composite test specimens with disperse spherical particles. Two sample types were made, including Modified Compact Tensile (MCT) specimens for dynamic fracture experiments, and Single Edge Notch (SEN) specimens for characterization of arrested cracks. The SEN specimens had the geometry shown in Figure 5, and the MCT specimens had the geometry shown in Figure 6.
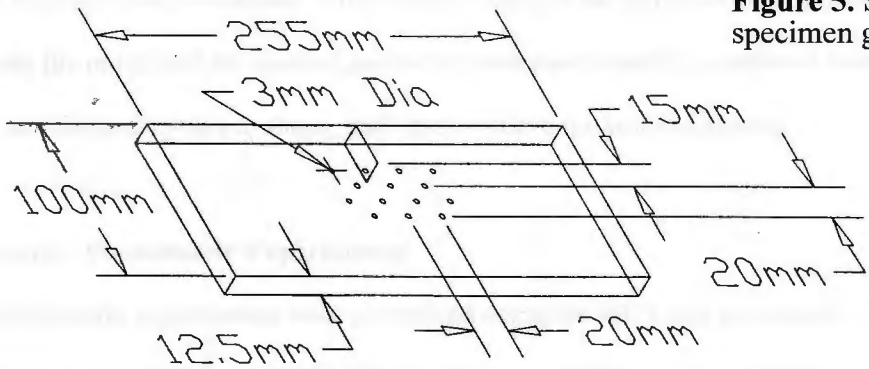
Figure 5. SEN specimen geometry

Figure 6. MCT specimen geometry
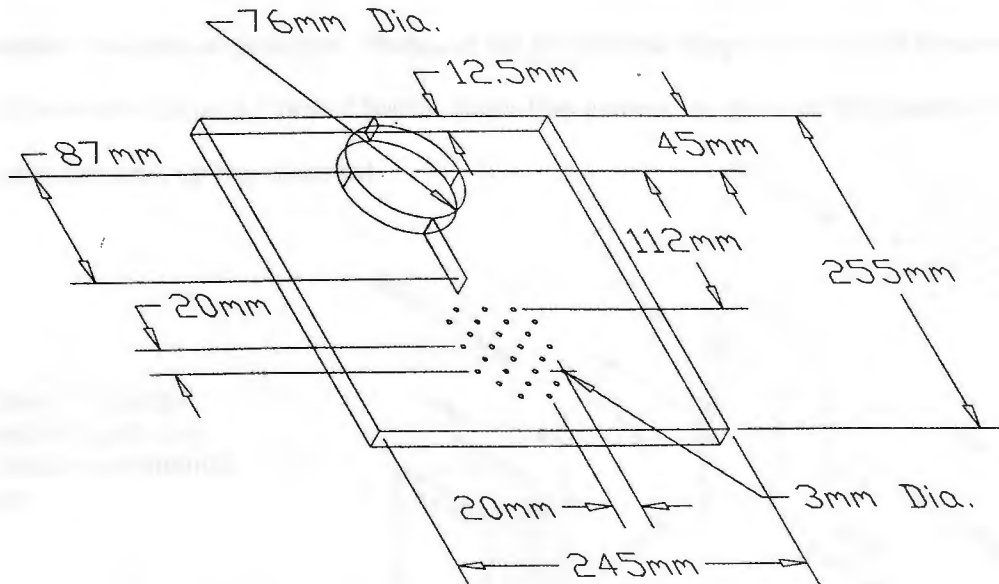
Test specimens of both types were prepared in an oversized, 300 mm long, by 315 mm wide, by 12 mm deep mold. The mold (lined with a Mylar film and coated with mold-release to ease sample removal) was first leveled on its side within +/- 0.4 mm of horizontal, after which a 6 mm deep layer of polyester was poured into the mold. At the beginning of gelation of this first layer of polyester, an arrangement of particles was made on the surface. While the first layer was still not fully cured, the mold was covered over (except one corner was left open to allow filling), and the mold was inclined to approximately 45°. The mold was then filled by pouring polyester in from the uncovered end. After initial curing of the polyester, the specimens were removed from the mold, and the desired geometry's were achieved by a series of machining operations, and thermal cycles to shape, and stress-relieve the test specimens.

4.10   Dynamic Photoelastic Experiments

Dynamic photoelastic experiments were performed using the MCT test specimens. The specimens were assembled into a loading fixture under conditions of fixed displacement loading. With this type of loading the dynamic crack is characterized by decreasing K_{ID}. Observation of the state of stress at the crack tip was achieved by positioning the loaded specimens in a circular polarizer. Photos of the photoelastic fringes at the tip of the advancing crack were taken using a Crantz-Chardin Spark-Gap camera. In this way the dynamic state of stress at the crack tip was observed.

Figure 7. Crantz-Chardin Spark-Gap Camera experimental setup
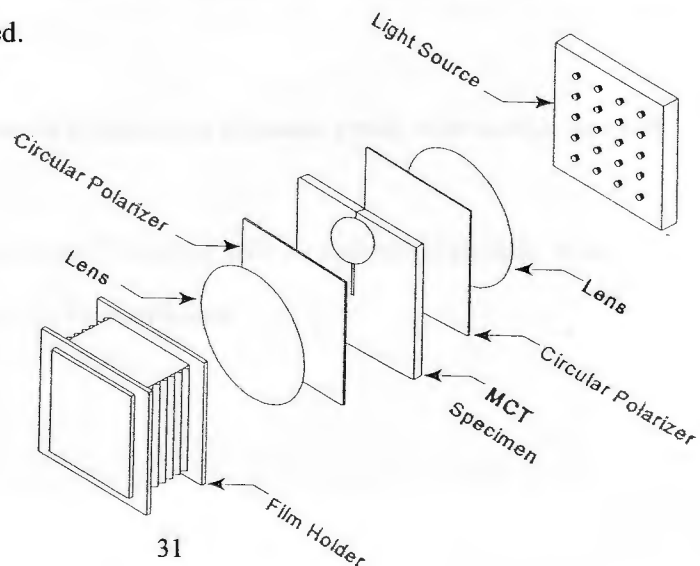
4.11   Test apparatus - dynamic experiments

In each dynamic experiment the MCT specimen was statically loaded to 150 pounds, using a hydraulically driven transverse wedge in a split-D fixture. This method of loading resulted in a predetermined stress intensity, K_{ID}, at the initially blunt crack tip prior to initiation of fracture. A solenoid-actuated knife was than used to initiate a dynamic crack in the specimen. The moving crack operated the Crantz-Chardin Spark-Gap camera by cutting a conductive film on the surface of the specimen, thereby triggering the camera just prior to progression of the crack past the first embedded particle.

Two groups of ten consecutive photographic images were taken in each experiment. By carefully measuring the elapsed time between each photo (approximately 5 microseconds), and the delay between the two groups of photos (approximately 20 microseconds), sequential photos of the dynamic crack in the area of 2 widely spaced particles were obtained during each MCT specimen experiment. The result was ten photos depicting the photoelastic state of stress at the tip of the dynamic crack as it approached, intersected, and exited the region of the embedded particles. Similar experiments were performed with specimens made with each of the three particle types.

4.12   Photographs of isochromatic fringes as a dynamic crack intersects a Buna-N particle

Photographs of the dynamic interaction of the crack with an embedded particle, in an experiment with Buna-N particles, can be seen below.

Figure 8. Photo 5/20 of isochromatic fringes as a dynamic crack intersects a Buna-N particle

Figure 9. Photo 6/20 of isochromatic fringes as a dynamic crack intersects a Buna-N particle

33
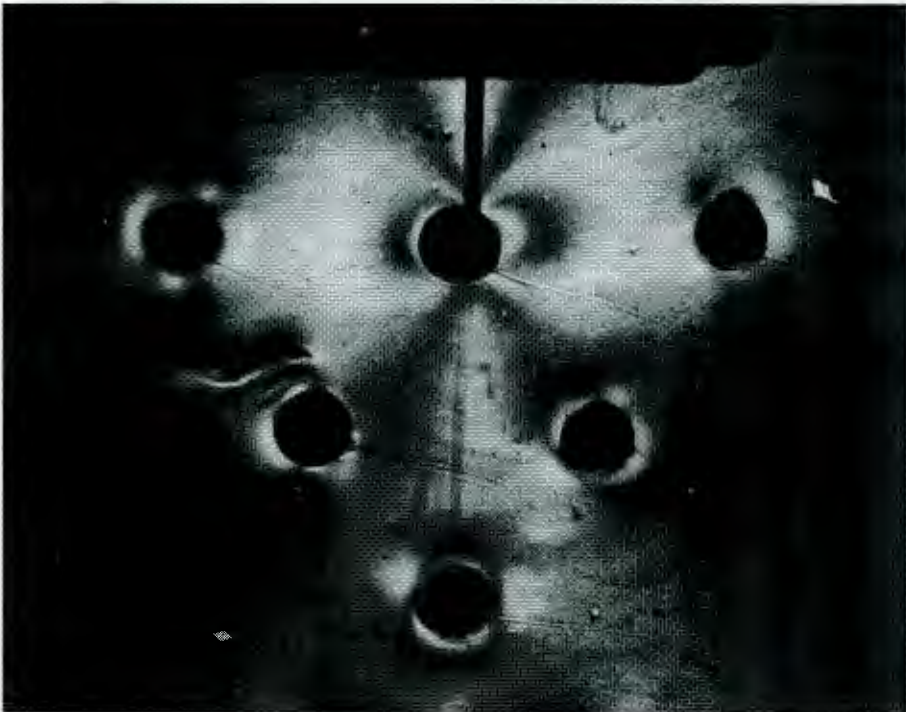
Figure 10. Photo 9/20 of isochromatic fringes as
a dynamic crack intersects a Buna-N particle

Figure11. Photo 12/20 of isochromatic fringes as
a dynamic crack intersects a Buna-N particle

Figure 12. Photo 14/20 of isochromatic fringes as a dynamic crack intersects a Buna-N particle
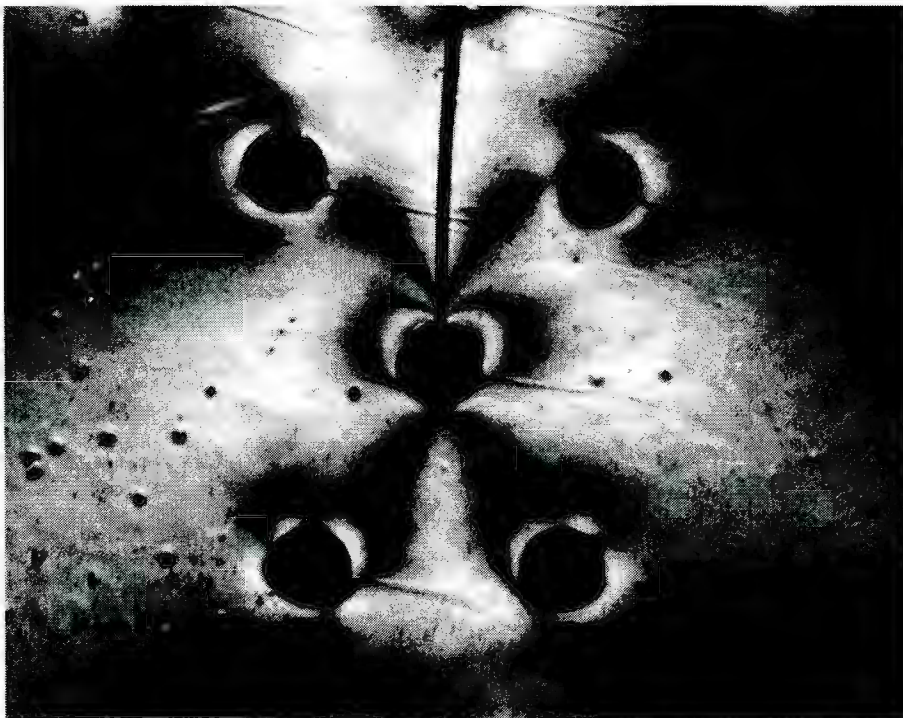
Figure 13. Photo 15/20 of isochromatic fringes as a dynamic crack intersects a Buna-N particle

4.13   Crack tip velocity

The trigger input that initiated the camera was also used as an input trigger to a digital

oscilloscope to begin a trace on the oscilloscope. Using a light detector at input "A" to the

oscilloscope, the elapsed time between sparks (and time between photographs) of the Crantz-

Chardin Spark-Gap camera was measured. By using the photographs to make dimensional

measurements of the crack advance from one photo to the next, and knowing the time elapsed

between photos, the crack velocity was determined. Velocity profiles are shown below in

Figures 14, 15 and 16 for dynamic cracks with Buna-N, glass and steel particles.

Figure 14. Crack Tip Velocity
Experiment 1 / Steel Balls

Ave. Velocity
264 m/sec

------- Particle boundaries
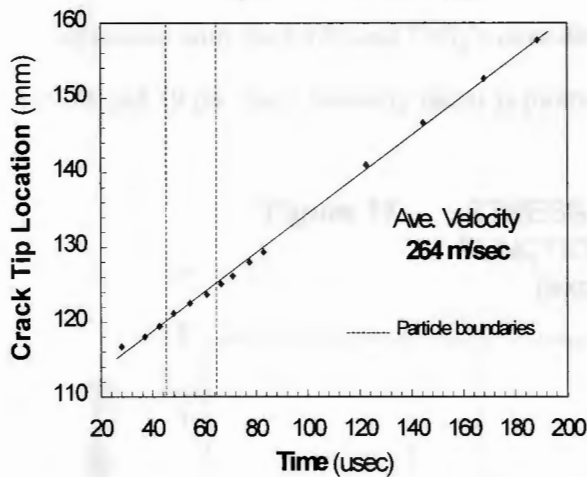
Figure 15. Crack Tip Velocity
Experiment 9 / Rubber Balls

Ave. Velocity
248 m/sec

------- Particles 1 + 2
Boundaries
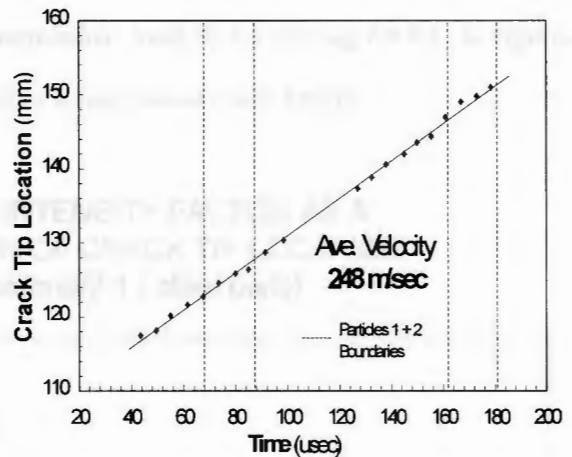
Figure 16. Crack Tip Velocity
Experiment 12 / Glass Balls

Ave. Velocity
252 m/sec

------- Particle boundaries

36
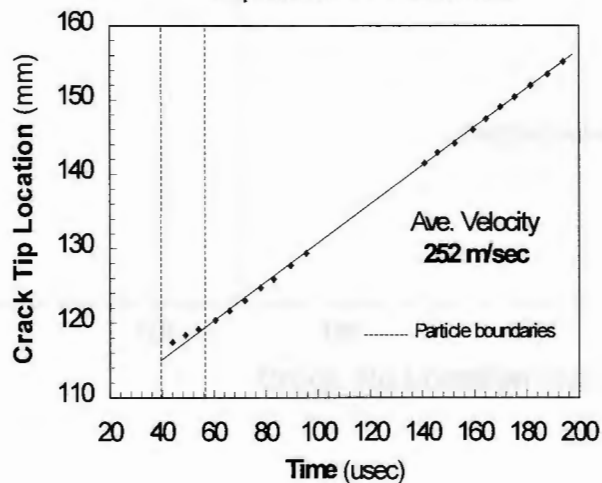
4.13   The dynamic stress intensity factor

The dynamic behavior of spherical particle reinforced brittle matrix composite materials was studied using the birefringent behavior of the 458-C polyester matrix. The twenty high speed still photographs of the advancing crack, obtained using the Crantz-Chardin Spark-Gap camera, captured the isochromatic fringes at the tip of the propagating crack. The fringes in the photos were then analyzed by digitizing the fringe order and location of points on fringes around the crack tip. This data was input to a computer program which computes the dynamic stress intensity factor using Irwin's solution for the dynamic state of stress at the crack tip, in combination with Sanford's and Dally's over-deterministic method for solving for K_I. In figures 17, 18 and 19 the stress intensity factor is plotted as a function of crack length.

Figure 17.   STRESS INTENSITY FACTOR AS A FUNCTION OF CRACK TIP LOCATION (experiment 1 / steel balls)
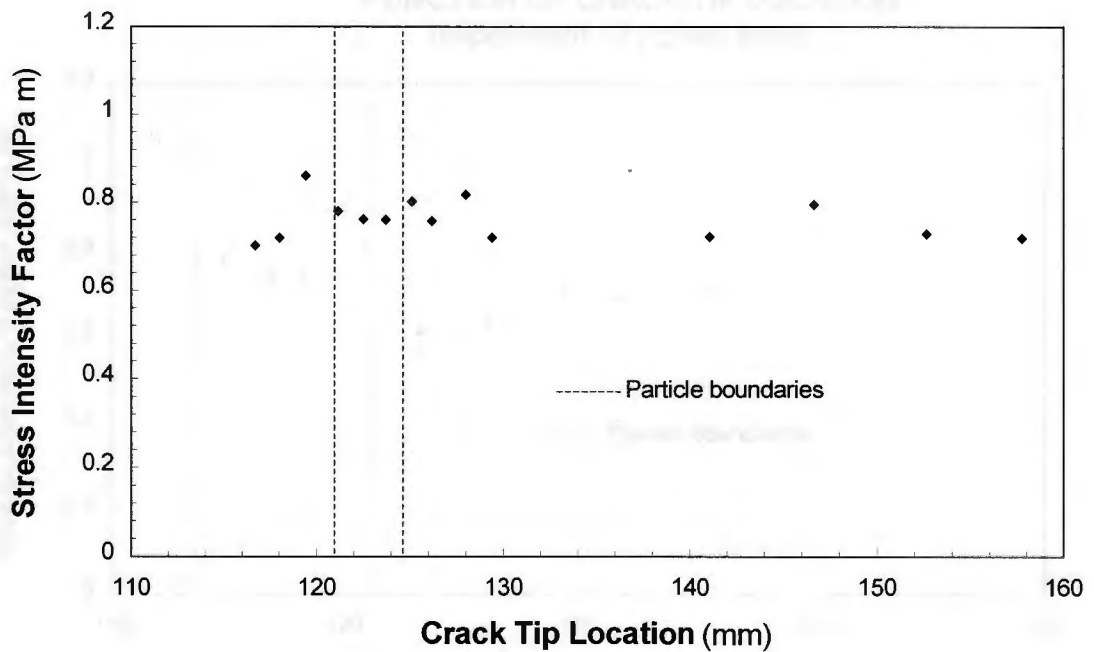
Figure 18. STRESS INTENSITY FACTOR AS A
FUNCTION OF CRACK TIP LOCATION
(experiment 9 / rubber balls)
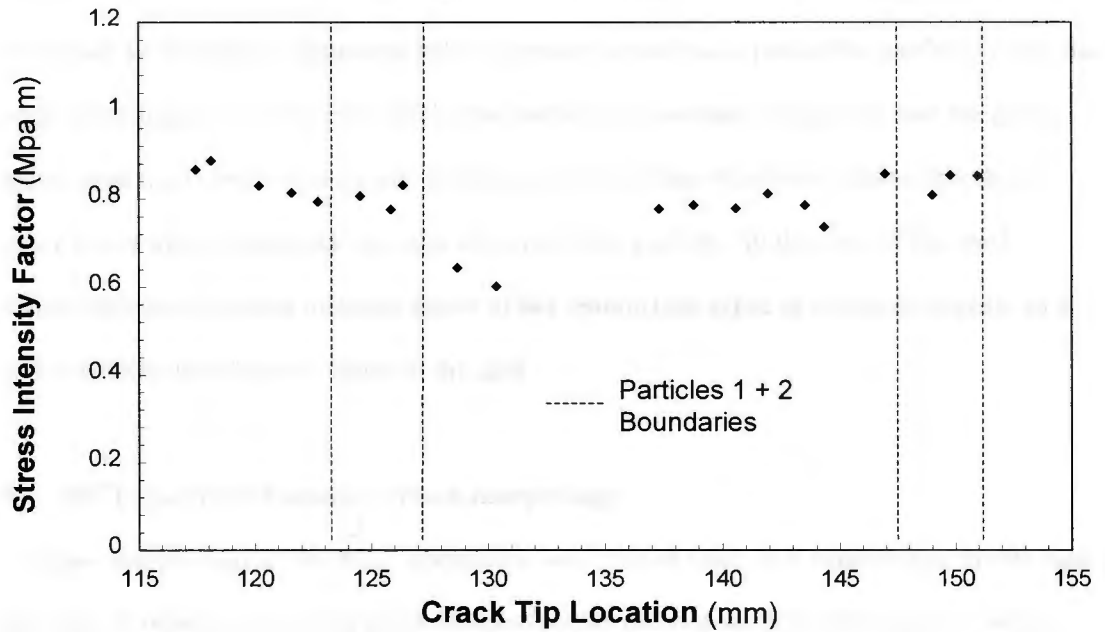
Figure 19. STRESS INTENSITY FACTOR AS A
FUNCTION OF CRACK TIP LOCATION
(experiment 12 / glass balls)

38
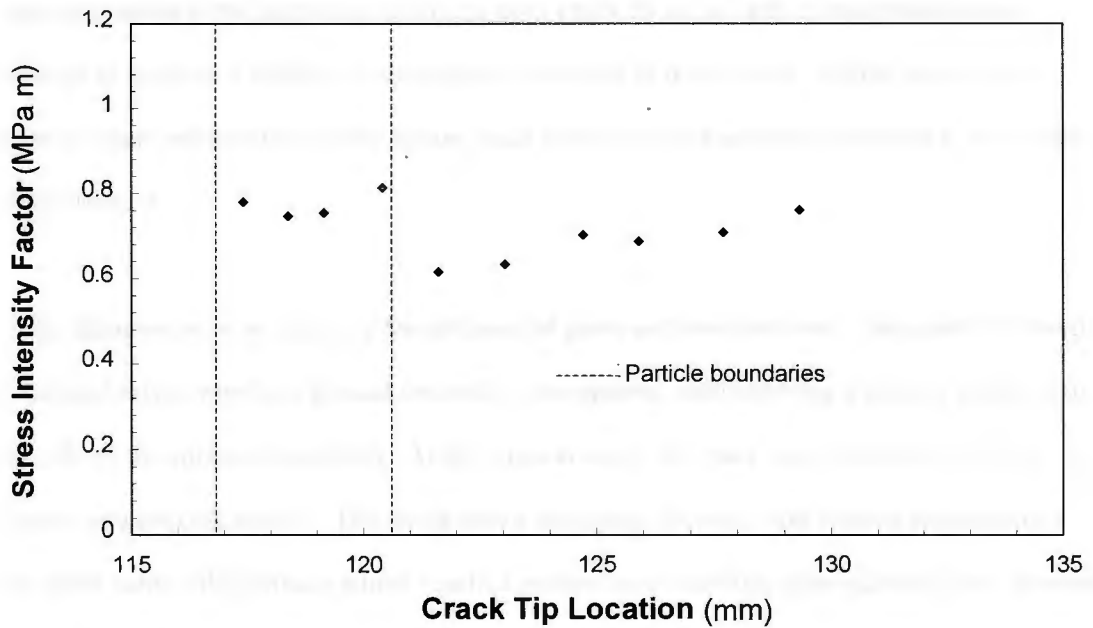
As can be seen in figures 17, 18 and 19 the apparent change in the stress intensity factor at the crack tip as it passes the embedded particles is small, except for the case of the glass particle which shows an increase of approximately 30 percent as the crack passes the particle. Also, the velocity of propagation of the crack tip by the particles is constant, except for near the glass particle where the velocity is reduced. In the case of the Buna-N rubber spheres, the stress intensity factor dips as the crack tip exits the area of the particle. In the case of the steel spherical particles the stress intensity factor either remains the same or increases slightly as it exits the particle, with higher scatter in the data.

4.15   MCT specimen fracture surface morphology

The surface morphology of the MCT specimens was studied after each experiment. In the case of the Buna-N rubber spheres the crack traveled across the mid-section of the sphere, with a distinct edge perpendicular to the rubber-polyester interface, with no apparent interruption in the crack's path. That is, the Buna-N rubber particles were circumvented by the planar crack. It was noted after the experiments with the Buna-N rubber that each of the rubber spheres remained bonded to the polyester matrix on both crack faces, in spite of the crack having advanced as much as 5 inches (40 diameters) past each of the spheres. Minor bowing was observed where reformation of the planar crack front occurred adjacent to the back side of the rubber particles.

A wake phenomena was observed for all cases of glass and steel spheres. The crack followed the hemispherical interface, around one half of the sphere, until reaching a critical angle on the back side of the spherical particles. At this critical angle the crack was diverted out of the interface and into the matrix. The result was a nonlinear (bowed), and angular (non-planar) crack front behind the particle which reached planar/linear stability approximately one diameter after the particle.

39

Figure 20. Crack surface morphology near a glass particle

Figure 21. Crack surface morphology near a steel particle

Crack arrest was observed in samples with glass spheres, and crack tip bowing to varying degrees was observed for all cases of glass and steel spheres in which separation of the hemispherical interface occurred.

Figure 22. Crack morphology and crack arrest near a glass particle
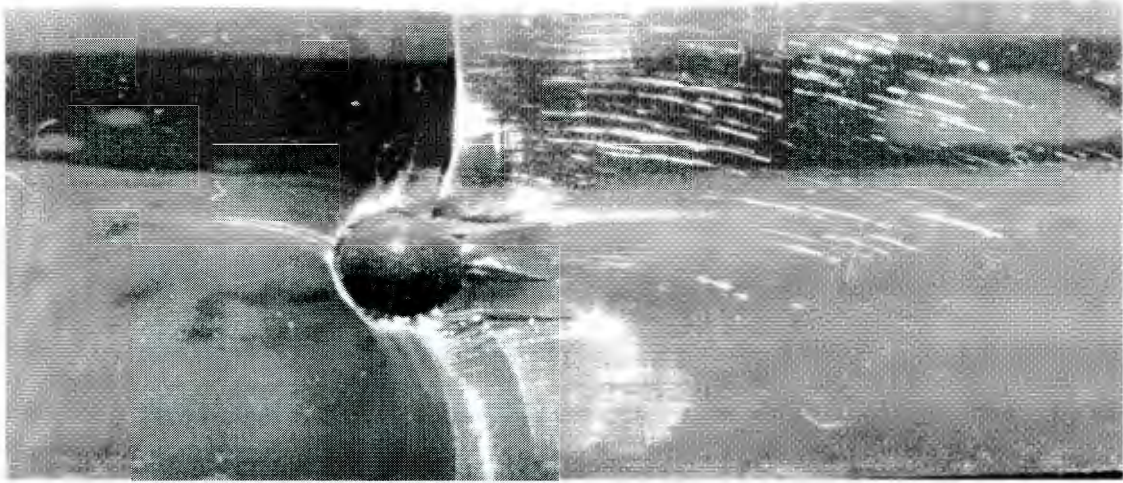
4.16   Arrested cracks near an embedded particle in a Modified Compact Tensile Specimen

The high-speed photos of dynamic cracks in MCT specimens show isochromatic fringes which represent the maximum in plane shear stresses τ_m in the field around the crack tip. While this data can be coupled to Irwin's stress field equations to solve for the stress intensity factor K_I , the resolution of the photos is not sufficient to clearly show details of the contour of the leading edge of the crack. The surface morphology of the tests specimens can be studied to deduce the shape of the leading edge of the crack, but the information gained from observing the cracked though specimens does not give complete information about the character of the crack tip.

Lee, Howard and Clegg [41] studied the nature of cracks arrested in close proximity to interfaces in order to learn about the process of deflection and arrest near interfaces. Their experimental methods included fracture of Single Edge Notch specimens. To study fracture behavior near bi-material interfaces they induced cracks to arrest in close proximity to the

interfaces. This same method has been used here to study the character of the leading edge of cracks in close proximity to embedded spherical particles.

Cracks were initiated in SEN specimens by loading a preformed crack on one edge using a sharp wedge and an arbor press while rigidly supporting the opposite edge of the specimen. By varying the load, specimens were obtained with cracks which arrested just prior to encountering the particles, as well as at all stages of progression past the particles. Photos of cracks near glass, steel and Buna-N rubber embedded spherical particles are shown below. The phenomena of uniform progression of the crack front past the Buna-N rubber particles can be seen. In the case of the steel and glass particles, accelerated progression of the crack through the particle-matrix interface over the poles of the particles can be seen, as well as retarded crack advance along the equator, and crack bowing in the matrix away from the particles.

4.17   Photographs of arrested cracks intersecting various particles in SEN specimens

Figure 23. SEN experiments with crack arrest just past a Buna-N rubber particle
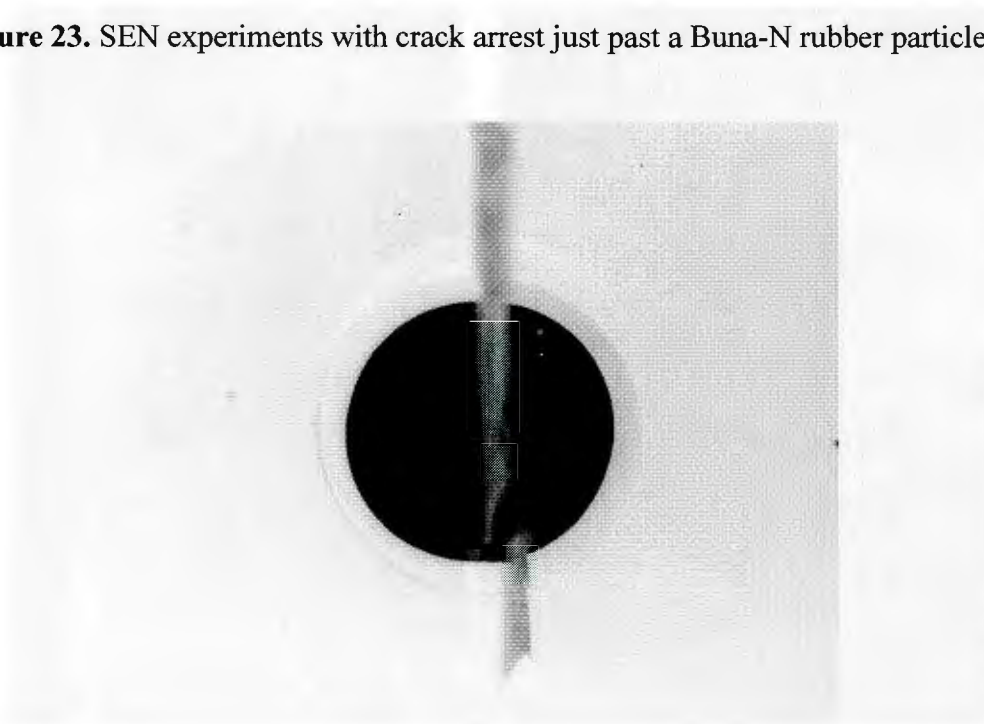
Figure 24. SEN experiments with crack arrest approaching a glass particle

Figure 25. SEN experiments with crack arrest intersecting a glass particle with beginning interface fracture on one hemisphere
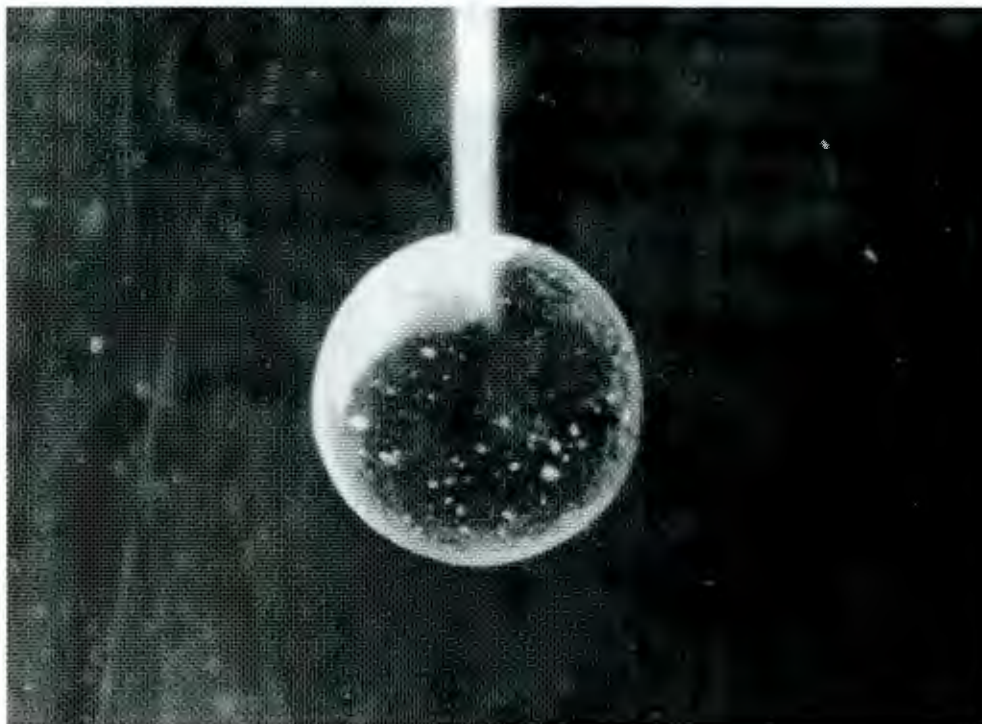
Figure 26. SEN experiments with crack arrest intersecting a glass particle with advanced interface fracture on one hemisphere
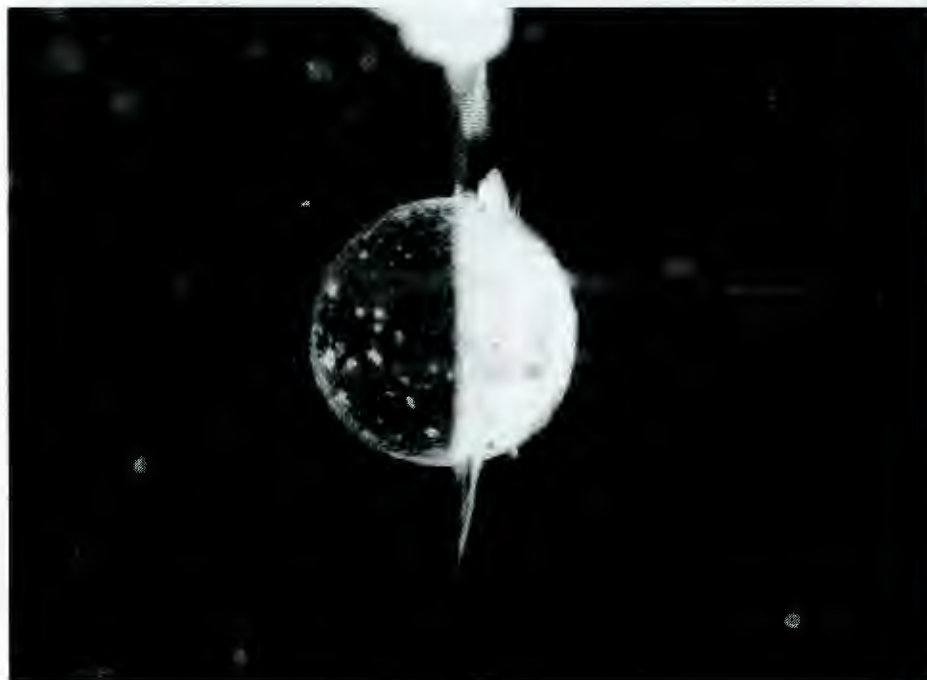
Figure 27. SEN experiments with crack arrest intersecting a glass particle with advanced interface cracking and crack tip bowing
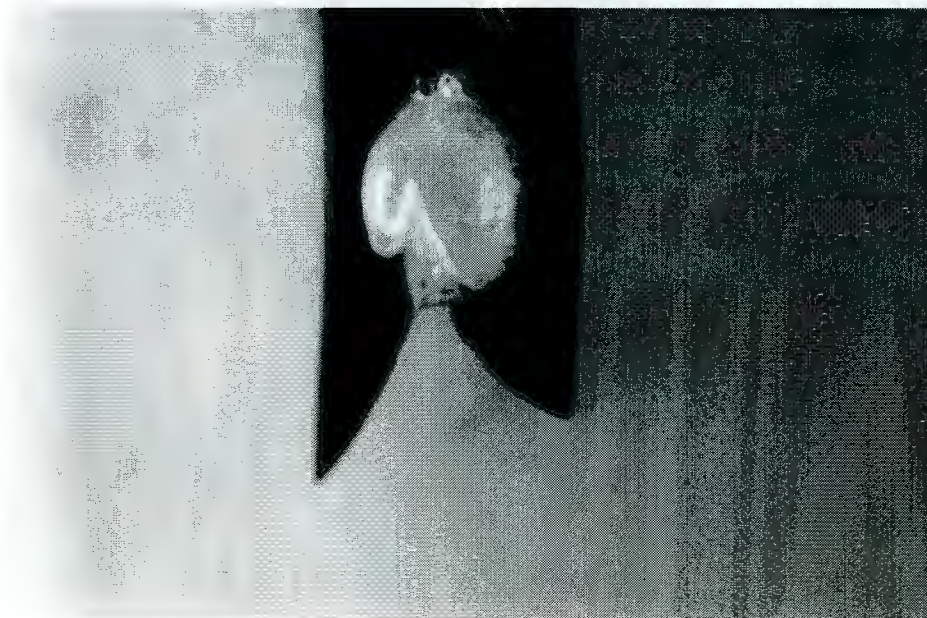
Figure 28. SEN experiments with crack arrest approaching a steel particle

Figure 29. SEN experiments with crack arrest intersecting a steel particle
with interface fracture on one hemisphere

The samples with glass and steel spheres had cracks with surface morphologies that were alike, and that were more complex than that of the Buna-N rubber spheres. Like the samples with Buna-N spheres, the advancing crack first intersected the glass or steel spherical particles at or near the equator of the particle (see figures 24 and 28), and then began to travel by the particle as a planar crack in the matrix. But, unlike the Buna-N crack trajectory, the leading edge of the crack in the matrix advanced at a slower velocity near the sphere than away from the sphere (crack tip bowing). Also, upon intersecting the glass or steel spheres, the crack progressed around the hemispherical particle-matrix interface, at the same time that it progressed through the matrix at the equator of the sphere. And, unlike the planar crack trajectory in the matrix around the Buna-N particles, the cracks in the matrix near the glass and steel spheres was not planar, and was instead deflected slightly towards the pole.

The leading edge of the hemispherical interface crack tips were continuous with the equatorial cracks, but the crack tip progression was faster over the pole of the sphere (see figures 25, 26 and 29) than near the equator. The second hemisphere of both the glass and steel spheres remained bonded across the interface, while separation occurred and the crack advanced along the first hemisphere.

46

CHAPTER V

PAPER

5.1   Crack propagation and damage mechanics in the area of a circular inclusion

Crack-particle interactions, and their relation to material fracture toughness, are important in many composite systems. Two examples of materials with enhanced properties imparted from embedded particles are metal-reinforced brittle ceramics with improved fracture toughness from the added ductile particles, and polymers with enhanced fracture toughness due to the addition of rubber particles. In each of these composite systems the crack-particle interactions play a defining role in characterization of the system material properties.

In the present work the interactions between an advancing crack in a brittle matrix, and spherical second phase particles embedded in the matrix, has been studied in order to learn the factors influencing the intrinsic fracture toughness of particle-filled brittle matrix composite systems. In particular, the present paper is focussed on the evolution of the crack front as it passes a single particle. Several fundamental aspects of crack-particle interactions are observed during the evolution of crack advance in these experiments. Crack advance is seen to include processes of crack deflection, crack-front bowing, crack face bridging, and crack path dependence on particle-matrix interface de-bonding. The role of matrix-particle elastic modulus mismatch, and the role of matrix-particle interfacial adhesion are seen to be parameters that largely define the path and shape of the advancing crack in the area of the embedded particles.

The crack front progression, and particle-matrix-crack tip interactions have been studied by a variety of techniques. These include static observations of arrested cracks that were induced in single edge notch specimens (SEN). In these experiments, the energy available at crack

initiation was varied, with the result that cracks were made to arrest at varying stages of interaction between the crack front and a spherical particle.

A series of dynamic experiments were also performed, using photoelastic techniques to make observations of a dynamic crack-front passing spherical particles in modified compact tensile specimens (MCT). The particle spacing and matrix material thickness was kept the same in both the SEN and MCT specimens, which allowed inter-comparison of crack propagation results. And finally, by observation of crack surface morphology in the area of the spherical particles (including an MCT specimen with a crack arrest event due to a bridged crack at a particle), it has been possible make several conclusions about crack-particle interactions. The mechanisms that contribute to a material's fracture toughness that have been investigated in this work are: crack deflection, crack tip bowing, crack arrest, crack bridging, and the relationship between interface strength and crack path selection. The purpose of the work has been to assess experimentally the size of the process-zone, the toughening contribution by the various mechanisms, and the role of the mechanical properties of each individual constituent phase.

5.2   Mismatch of particle/matrix elastic modulus

An elastic modulus mismatch between particles and the matrix is known to result in uneven stress distribution around the circumference of the embedded particles. Eshelby [44] developed a closed form solution for the state of stress inside a particle in an isotropic material under a remote stress as follows:

$$\sigma_{xx}^{in} = \sigma_{yy}^{in} = \frac{1}{3}\left[\frac{\kappa_1}{\delta_0(\kappa_1 - \kappa_0) + \kappa_0} - \frac{\mu_1}{\varphi_0(\mu_1 - \mu_0) + \mu_0}\right]\sigma_{zz}^0$$

$$\sigma_{zz}^{in} = \left[\frac{2}{3}\frac{\mu_1}{\varphi_0(\mu_1 - \mu_0) + \mu_0} + \frac{1}{3}\frac{\kappa_1}{\delta_0(\kappa_1 - \kappa_0) + \kappa_0}\right]\sigma_{zz}^0$$

where κ_1, μ_1, κ_0 and μ_0 are the bulk and shear modulii of the particle and the matrix respectively, and

$$\varphi_0 = \frac{(1 + \nu_0)}{3(1 - \nu_0)} \qquad\qquad \delta_0 = \frac{2(4 - 5\nu_0)}{15(1 - \nu_0)}$$

with ν_0 being Poisson's ratio of the matrix.

By fabricating composites using Buna-N rubber particles with elastic modulus less than the polyester matrix material ($E_{buna}/E_{matrix} < 1$), and using Glass and steel particles with elastic modulus much higher than the polyester matrix ($E_{steel/glass}/E_{matrix} \gg 1$), the effect of elastic modulus mis-match on the path of a dynamic cracks in a particle-matrix composite was studied. Depicted below in figures 30a and 30b are the locations of stress concentrations near embedded particles for the case of elastic moduli of the particle higher than the composite matrix material ($E_{particle}/E_{matrix} \gg 1$ such as with Glass or steel), and lower than the matrix material ($E_{particle}/E_{matrix} < 1$ such as with Buna-N rubber), under conditions of remotely applied loading, as was the case in these experiments

Figure 30. Locations of stress concentrations, and possible fracture paths, near embedded particles for the case of elastic modulii of the particle higher than, and lower than, the composite matrix material ($E_{particle}/E_{matrix} > 1$ such as with Glass or steel, and $E_{particle}/E_{matrix} < 1$ such as with rubber). The arrows show loading. [reproduced from 47 p2213]

$E_{particle}/E_{matrix} > 1$

Stress concentrations around
and within the particle

$E_{particle}/E_{matrix} < 1$

Tangential stress concentration
around the particle
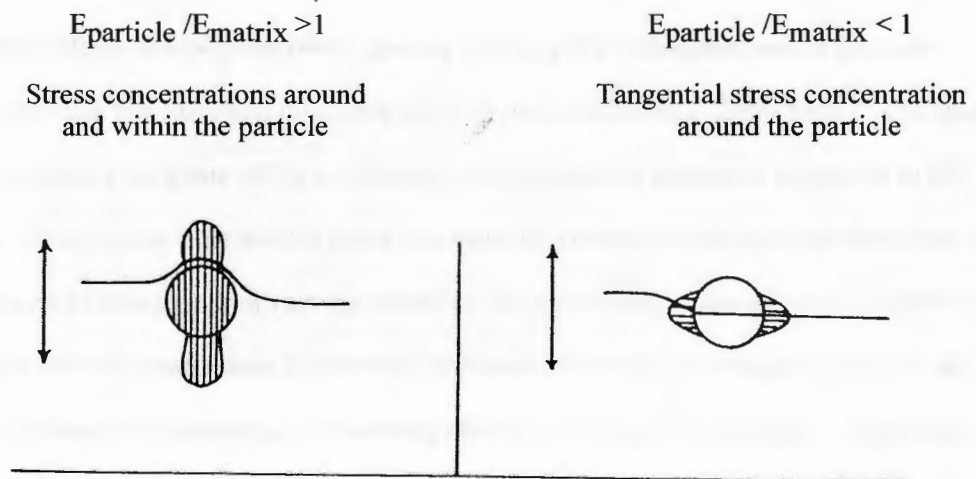
As can be seen in figures 26 and 29 above, the crack propagation paths near the steel and glass particles were similar, while, as can be seen in figure 23, the crack propagation path near the composite with Buna-N rubber particles was quite different. The path of cracks in the polyester matrix near the low modulus rubber particles was along the mid-plane of the particles, with crack fronts that were planar and linear. These low modulus rubber particles remained intact, and bridged the crack faces, by remaining bonded to the matrix along the embedded hemispheres on both crack faces. The two hemispherical matrix-particle interfaces continued to remain bonded to the opposing crack faces long after the crack had progressed by the particle.

In the case of the high modulus glass and steel particles, the crack front exhibited a nonlinear progression as it advanced both through the matrix on each side of the particle (nearly planar, nonlinear matrix crack front), while at the same time progressing along the hemispherical particle-matrix interface (highly nonlinear hemispherical interface crack). The crack paths reformed as a planar linear crack approximately one diameter past the particles. As can be seen in figures 20 and 21 above, crack tip bowing and out of plane crack deflection were observed for both steel and glass particles, and in the case of glass particles, figure 22 above, crack arrest was also observed.

5.3 Effects from crack-to-particle spacing (crack path deflection near a particle)

In the present work the specimen thickness was 4 particle diameters (12mm/3mm). The space between particles in the plane of the specimens was four particle diameters or greater in all directions. During these experiments cracks intersected particles on the particle centerline, off-center, and cracks also passed at varying distances "near particles". That is, cracks passed by particles at distances greater than 2 diameters (minimal effect on crack trajectory) and at all distances less than two diameters, with varying effects on crack path trajectory. Cracks that passed particles at a distance of 1 diameter or less from the particle, but without intersecting the

particle, showed evidence of a significant non-uniform strain field around the particle. This was observed as non-planar crack faces as shown in figure 31 below. In the case of cracks that passed at a distance of 2 diameters away from particles or greater there was no observable deflection of the crack face. Moschovidis and Mura [45] showed, in a numerical result for the problem of two ellipsoidal inhomogeneities in an infinite solid, that interactions between inhomogeneities become negligible at radial spacings of Δ/a greater than 4, where a is the inhomogeneity diameter, and Δ is the center-to-center spacing. Xiao and Pae [46] obtained a similar result for the case of a spherical particle near a penny shaped crack. Therefore, the trajectories of dynamic cracks near the steel and glass particles in the attached photos, are consistent with the numerical solutions of Moschovidis and Mura, and Xiao and Pae.

Figure 31. Crack surface morphology near a rubber particle showing a non-planar crack path. Spacing is approximately 2/3 particle diameter from the particle.

5.4   Thermal expansion coefficient mismatch

Another material property mismatch that had a bearing on crack propagation paths is the thermal expansion coefficient mismatch which caused residual stresses due to cooling from the elevated curing temperatures during specimen fabrication.   For the case where a spherical particle is embedded in an infinite medium, the stresses in the matrix at a distance r from the center of the particle are given by Miyata and Jinno as [47]:

$$\sigma_{rr} = -\beta(R/r)^3 \qquad \text{and,} \qquad \sigma_{\theta\theta} = \beta/2\ (R/r)^3$$

with:

$$\beta = \frac{(\alpha_m - \alpha_p)\Delta T}{\left[\dfrac{1 + \nu_m}{2E_m} + \dfrac{1 - 2\nu_p}{E_p}\right]}$$

where σ_{rr} and, $\sigma_{\theta\theta}$ are radial and tangential stresses, respectively, α is the thermal expansion coefficient (see table 3) ΔT is the cooling range and R is the particle radius. Figure 32 depicts residual thermal stresses around particles that are the result of particle and composite matrix materials with different thermal expansion coefficients ($\alpha_{particle} \neq \alpha_{matrix}$) cooling from elevated temperatures, for the case of $\alpha_{particle}/\alpha_{Matrix} > 1$ (Buna-N rubber), and for $\alpha_{particle}/\alpha_{Matrix} \ll 1$ (glass < steel << polyester).

Figure 32. Residual stresses, and possible fracture paths, near embedded particles for the case of thermal expansion coefficient α of the particle higher than, and lower than the composite matrix material ($\alpha_{particle}/\alpha_{matrix} > 1$ such as with rubber, and $\alpha_{particle}/\alpha_{matrix} < 1$ such as with Glass or steel). [reproduced from 47 p2211]
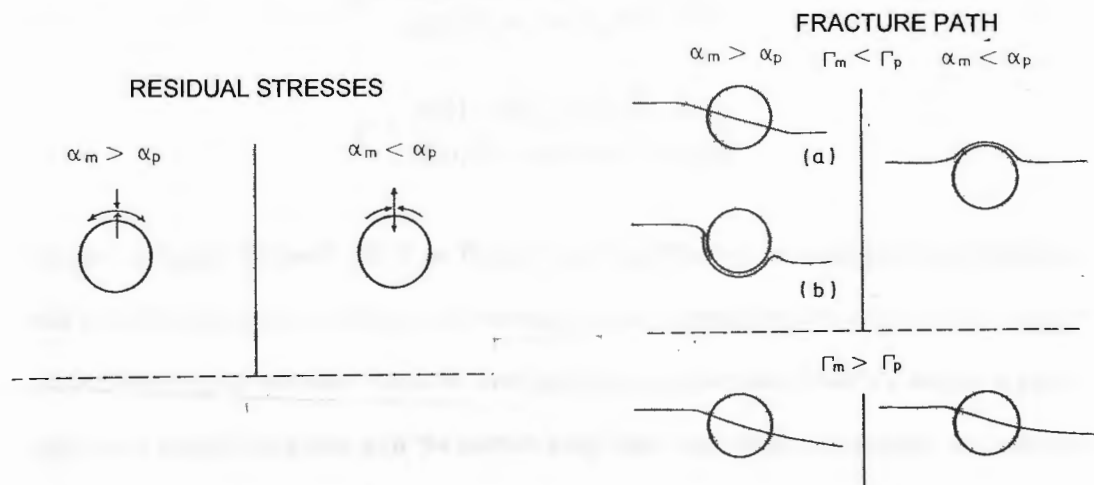
5.5   Crack path as a function of mixed mode loading at the particle matrix interface

In these experiments the high modulus particles became unbonded as the crack moved by the particles. The mode of crack advance was by progressive failure at the particle matrix interface. The degree of adhesion of the matrix to the high modulus particles was such that the through-thickness crack front advanced with varying velocity, and in preferential directions, along the particle-matrix interface. Evans, He, Hutchinson and Dalgleish [39] have postulated that the crack trajectory is dictated by the mixed mode loading phase (ψ = function of the ratio shear mode versus tensile mode loading), and by the relative fracture toughnesses of the materials at the interface. Evans et al. define the loading phase angle ψ as:

$$\psi = \tan^{-1}(\upsilon/u) - \varepsilon \ln r - \tan^{-1} 2\varepsilon$$

where r is the distance from the crack tip, and υ and u are the relative shear and opening displacements, and with

$$\varepsilon = \frac{\ln[(1-\beta)/(1+\beta)]}{2\pi}$$

53

where Dundurs' parameters α and β are given by:

$$\alpha = \frac{\mu_1(1-\nu_2) - \mu_2(1-\nu_1)}{[\mu_1(1-\nu_2) + \mu_2(1-\nu_1)]}$$

$$\beta = \frac{\mu_1(1-2\nu_2) - \mu_2(1-2\nu_1)}{2[\mu_1(1-\nu_2) + \mu_2(1-\nu_1)]}$$

Depicted in figures 33a and 33b from Evans' et al.'s [39] work are predictions of interface crack path directions for materials with varying elastic modulus mismatches. In the case of particles with higher modulus (such as steel and glass, in polyester matrix), negative phase angles exist around the equator of the particles (ψ from high shear component, and negative sign from particles with modulus higher than matrix).

Figure 33. Predicted fracture paths for mixed mode loading conditions with various material property mismatches. With positive ψ defined by mode II arrow directions. [reproduced from 39 p3251]

a) The region of interface cracking for three values of elastic mismatch

b) The region of interface cracking for materials with different fracture toughness
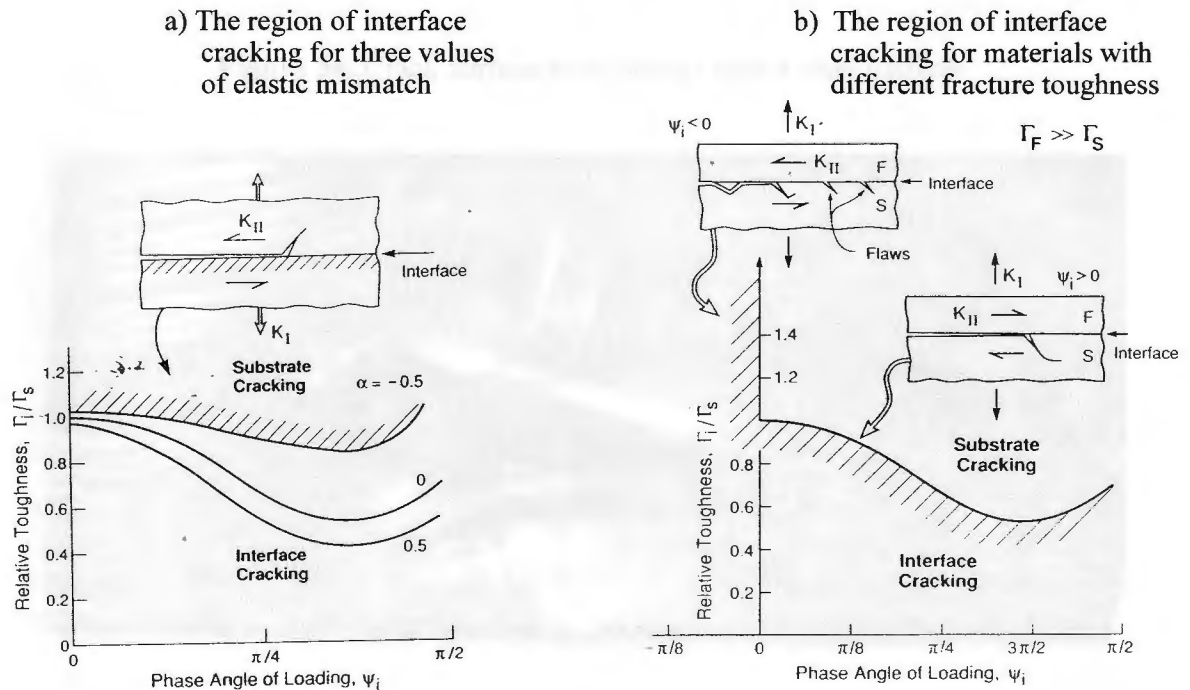
In the case of cracks advancing past spherical particles with higher modulus than the matrix, the hemispherical geometry of the crack-particle interface results in variations in the degree of mixed mode loading along the crack front. This is seen in the interface cracks of the steel and glass particles in the experiments reported here. As the crack tip passes over the pole of the particle (on the centerline of the steel and glass particle/MCT specimens), the crack front accelerates into a region of tensile loading. At the same time, in the region of the matrix on either side if the particle (away from the particle, towards the outside surfaces of the MCT specimen), the loading is also tensile. But, in the region between the equator of the particle and the pole of the particle, there is a sharp transition from the remote tensile loading in the matrix, to highly mixed mode loading at the equator, and back to tensile loading over the pole of the particle. It is this variation in relative shear mode υ, and opening mode μ loading ($\psi = f(K_I / K_{II})$) at the interface crack tip that explains the variation in crack front profile seen previously in figures 20 to 22, figures 24 to 29 and below in figure 34. Each of these figures depicts the stages of crack advance, as well as the bowing that occurs in the matrix near the particle.

Figure 34. Crack surface morphology near a steel particle
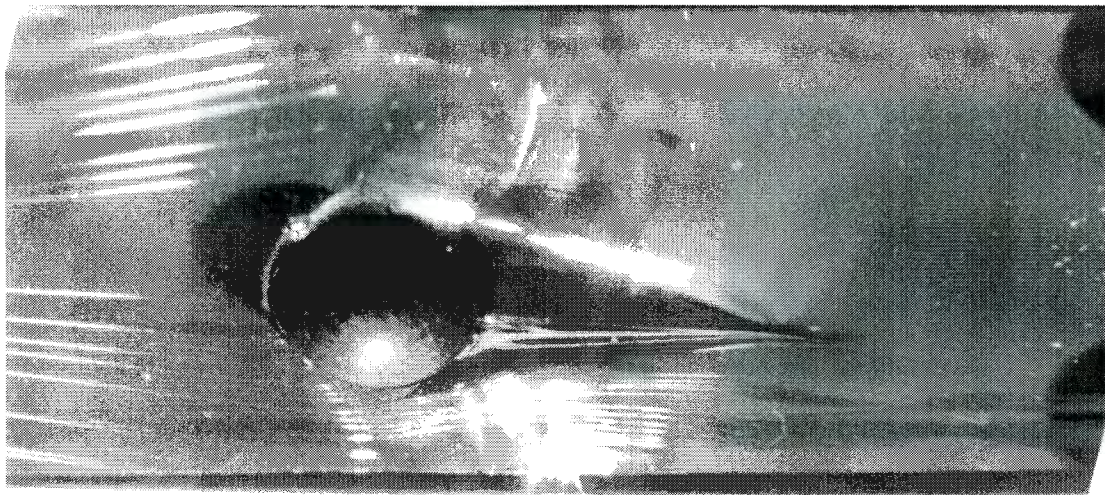
As can be seen in figure 34, as the crack progresses towards the back edge of the particle, a V-shaped stepped surface is formed as the crack exits the particle-matrix interface. This is due to a transition from tensile loading over the pole of the particle, to mixed mode loading behind the pole. At the same time the two arms of the crack front close to the equator (in mixed mode loading) coalesce with the out of plane interface crack exiting the pole, forming a non-planar crack purely in the matrix. Approximately one diameter past the particle the crack front has reformed as a linear and planar crack.

5.6   Correlation of crack tip bowing with the perturbation analysis models of Rice, Gao, Bower, Ortiz, and Pezzotti et al.

In addition to the crack tip variations noted above, crack arrest and out of plane crack deflection were also observed. These observations of the morphology at the crack tip can be correlated to the recently developed concepts for the fracture toughness enhancement associated with crack tip pinning and crack tip bowing from embedded particles reported in the introduction. Lange hypothesized that in the case of cracks with crack tip bowing due to pinning from dispersed inhomogeneities, "... the increment of energy absorbed (ΔU) for an increment of crack extension (ΔC) can be divided into two parts, i.e. one part (ΔU_S) associated with the energy to form new surface area and one part (ΔU_l) associated with the energy to form the increased length of the crack front." [28 p987].

Rice proposed a numerical model for stable variations in the shape of a crack front due to variations in stress intensity along the crack front from, for example, "...microscale heterogeneities when a crack tip begins to advance by and surround a fracture-resistant zone of material." [33 p575]. Rice also proposes that Lange's model for energy absorption mechanisms, solely from formation of new surface area, is an oversimplification of true

dynamics at the crack tip. Gao and Rice [8] went on to model cracks trapped by arrays of obstacles for the case of obstacles with toughness up to 4 times the matrix toughness. They described their numerical methods as purturbation analysis. Numerical results from the model are depicted below in figure 35 and figure 36.

Figure 35. The shape of a semi-infinite crack as it bypasses a single row of obstacles. [reproduced from 6 p836]
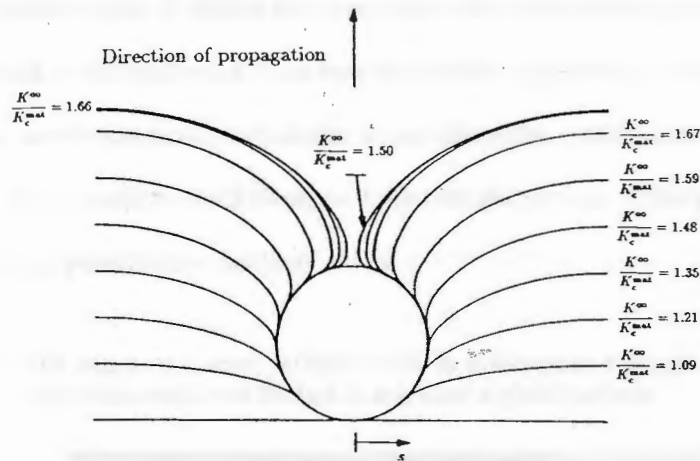
Figure 36. The variation of stress intensity factor around a crack front shown in figure 35. [reproduced from 6 p836]
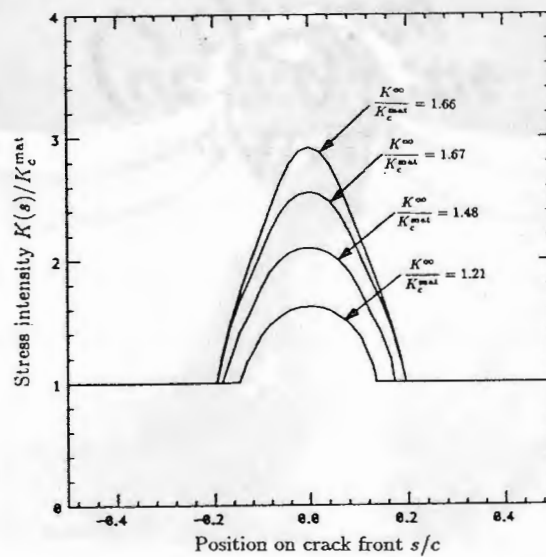
These curves are modeled after crack front bridging where the fracture toughness of the bridging element is greater than that of the matrix, and is a constant across its cross-section. As a result, the bridging particle either remains intact as the crack front passes, or the resulting fracture of the bridging element is behind the more advanced (bowed) crack front on either side of the bridging element.

It can be seen in figure 37 below that when the crack front bowing profiles described above are superimposed on the real crack front bowing of these experiments, that the shape of the crack front in the matrix has evolution similar to the case of the puturbation analysis. This is in spite of a much more complex crack front evolution inside the area of the particle-matrix interface than that of the purturbation analysis model.

Figure 37. The shape of a semi-infinite crack as it bypasses a single row of obstacles superimposed over bowed crack near a glass particle.
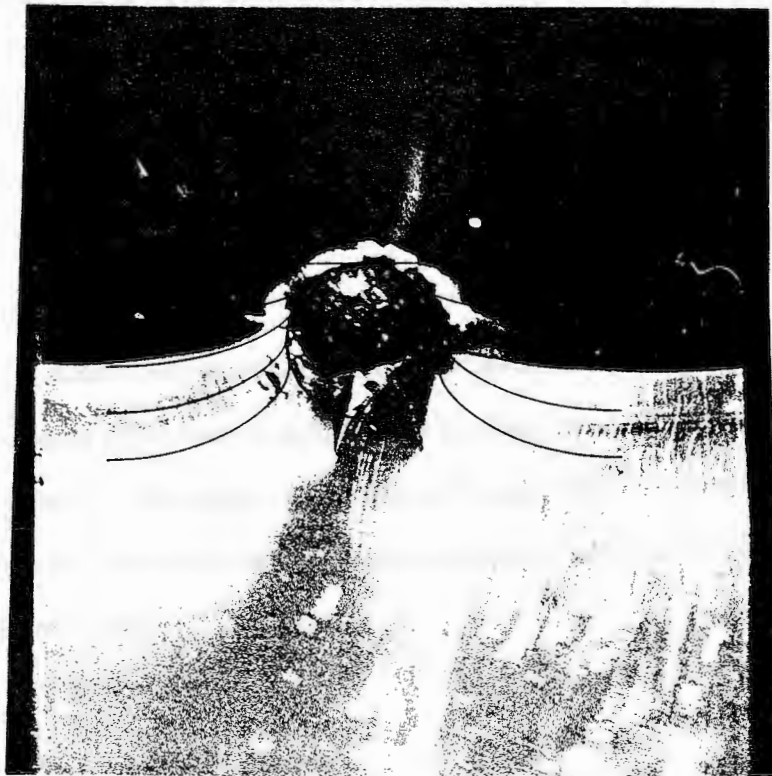
CHAPTER VI

CONCLUSIONS AND RECOMMENDATIONS

The only studies known to this author, involving dynamic fracture mechanics in the area of embedded particles, include a series of experiments that employed the method of caustics to study stress intensity factors during crack-particle interactions [15,16], and a series of experiments that employed low temperatures to obtain slow, stable crack progression past particles [14]. A new series of experiments have now been performed using photoelastic techniques and the birefringence of a brittle polyester matrix with embedded spherical particles, to study the interactions between dynamic cracks and embedded spherical particles. The study using caustics to measure stress level employed single edge notch specimens having particle diameters equal to the thickness of the specimen. With particle diameters equal to the thickness of the specimen the fracture experiments are more representative of a through thickness defect in a flat plate, than that of a spherical particle embedded in a matrix. In the present study, difficulties associated with fabrication of a specimen with embedding particles inside a matrix with material thickness greater than the particle diameter, have been overcome. The present study is of dynamic crack propagation in the area of particles with diameters of 1/4 to 1/3 the overall thickness of the matrix.

The stress induced birefringence of the polyester matrix allowed photoelastic observation of dynamic stresses at the crack tip during crack propagation. Modified compact tension specimens (MCT), 12mm thick, with 3.97mm diameter spherical particles spaced approximately 6 diameters apart on the mid-plane of the specimen were used in the dynamic fracture experiments.

59

By fabricating composites using Buna-N rubber particles with elastic modulus less than the polyester matrix material, and using Glass and steel particles with elastic modulus much higher than the polyester matrix, the effect of elastic modulus mis-match on the path of a dynamic crack in a particle-matrix composite has been studied.

It was found in fracture experiments with low modulus rubber particles that the path of cracks were through the mid-plane of the particles, with crack fronts that were planar and linear. Also, the Buna-N rubber particles bridged the crack faces by remaining bonded to the matrix on hemispheres on each crack face. These hemispheres remained bonded to the opposing crack faces long after the crack had progressed by the particle. The net stress intensity factor, observed as birefrigent fringes of the through thickness crack tip, was briefly reduced as the crack exited the vicinity of the Buna-N rubber particle. The average velocity of crack propagation was constant, although fringe tilt, which is an instantaneous indication of crack tip acceleration was observed as the crack exited the particle.

The high modulus steel particles became unbonded along one hemisphere as the crack progressed by the particles, by progressive failure at the particle matrix interface. The degree of adhesion of the matrix to the high modulus steel particles was such that the crack advanced with varying velocity, and in preferential directions, along the particle-matrix interface according to the mixed mode loading phase ($\psi = K_I / K_{II}$). A small degree of crack tip bowing was observed, as well as out of plane crack deflection. The net through thickness crack tip stress intensity factor showed small variations, due to the compounded effect of retarded crack advance at the periphery of the particle, and accelerated crack advance across the pole of the particle. As with the Buna-N rubber particles, the average velocity of crack propagation past

60

the steel particles was nearly constant, although fringe tilt, which is an instantaneous indication of crack tip acceleration was observed as the crack exited the particle.

Like the steel particles, the high modulus glass particles became unbonded along one hemisphere as the crack progressed by the particles, by progressive failure at the particle matrix interface. Again, like the steel particles, the degree of adhesion of the matrix to the high modulus particles was such that the crack advanced with varying velocity, and in preferential directions, along the particle-matrix interface according to the mixed mode loading phase ($\psi = K_I / K_{II}$). Crack tip bowing was more pronounced in the case of the glass particles and crack arrest were observed, as well as out of plane crack deflection. Unlike the steel particles, the glass particles showed a more distinct, approximately 30% increase in the net through thickness crack tip stress intensity factor, as well as a reduction in crack tip velocity. Like the steel particles, there was retarded crack advance at the periphery of the particle, although this effect was more pronounced in the glass particles. Also, there was accelerated crack advance across the pole of the particle.

In order to better understand the nature of the crack-particle interactions observed as fringe patterns in the dynamic experiments, additional studies were performed using Single Edge Notch specimens. Cracks were induced to arrest near the embedded particles. This allowed an approximate determination of the shape of the crack front, which was then correlated to the stress intensity factor and crack velocity.

One of the outcomes of the work reported above, is that it makes it possible to recommend several avenues for continued study of the interactions of crack fronts near embedded spherical particles in brittle polyester matrix materials. First, the particles studied in this investigation have elastic modulus either much lower than the matrix material (Buna-N particles), or many

61

orders of magnitude higher than the matrix materials (glass and steel). And, due to either the particles high elongation (Buna-N), or due to toughness that was higher than the matrix materials (glass and steel), none of these particles fractured as a result of progression of the crack by the particles. A possible means to achieve higher overall composite toughness in particle filled composites is to use particle materials with elastic modulus nearly equal to the matrix materials, but with higher toughness, such as with Lexan spherical particles. In future experiments, by using particles with elastic modulus nearly equal to the matrix materials, the path of the crack would not be deflected by unequal strain, and the associated stress concentrations at the matrix-particle boundaries would be reduced prior to cracking. Also, the tougher materials would tend to resist cracking, possibly resulting in crack trapping behavior that could be observed in the MCT photoelastic experiments.

Second, the effect from interfacial adhesion between the polyester matrix and the glass particles is believed to have been an important factor affecting the interactions of the cracks and particles. In these experiments there was moderately increased fracture toughness near the glass particles. This slightly increased toughness is consistent with predictions in the literature for enhanced toughness from crack tip deflection around particles. Additional work could be performed to study the effect from varying interfacial adhesion.

And third, the effect on fracture toughness from the interaction of one Buna-N particle with the advancing crack, which was seen in these experiments as a reduction in fracture toughness as the crack exited the area of the particle, could be studied and compared to predictions in the literature. The mitigating influence from bulk modulus effects as the crack first intersects the Buna-N particles, coupled with the near perfect adhesion and 300% or greater elongation of the Buna-N materials, have a role in the resulting fracture toughness. These influences, as well as the effect from increased particle density, could also be studied as part of continuing work.

62

LIST OF REFERENCES

1. Anderson, T.L., 1991, Fracture mechanics fundamentals and applications, CRC Press Inc, Boca Raton, Florida

2. Agarwal, B.D., Broutman, L.J., 1990, Analysis and performance of fiber composites, John Wiley & Sons Inc, New York

3. Pezzoti, G., Okamoto, Y., Nishida, T., Sakai, M., 1996, *On the near-tip toughening by crack-face bridging in particulate and platelet-reinforced ceramics*, Acta Metallurgica et Materialla, Vol. 44 no. 3, p899-914

4. Evans, A.G., Budiansky, B., Amazigo, J.C., 1988, *Small-scale crack bridging and the fracture toughness of particulate-reinforced ceramics*, Journal of the Mechanics and Physics of Solids,Vol. 36 no. 2 p167-187

5. Cox, B.N., Marshall, B.N., 1994, *Concepts for bridged cracks in fracture and fatigue*, Acta Metallurgica et Materialla, Vol. 42 no. 2 p341-363

6. Bower, A.F., Ortiz, M., 1991, *A three-dimensional analysis of crack trapping and bridging by tough particles*, Journal of the Mechanics and Physics of Solids, Vol. 39 no. 6 p815-858

7. Bower, A.F., Ortiz, M., 1993, *An analysis of crack trapping by residual stresses in brittle solids*, Journal of Applied Mechsanics Vol. 60 p175-182

8. Rice, J.R., Gao, H., 1989, *A first-order perturbation analysis of crack trapping by arrays of obstacles*, Journal of Applied Mechanics, Vol 56 pp 828-836

9. Evans, A.G., Faber, K.T.,1983, *Crack deflection Processes: I Theory*, Acta Metallurgica et Materialla, Vol. 31 no. 4, p565-576

10. Evans, A.G., Faber, K.T.,1983, *Crack deflection Processes: II Experiment*, Acta Metallurgica et Materialla, Vol. 31 no. 4, p577-584

11. Pezzotti, G., 1993, *On the actual contribution of crack deflection in toughening platelet-reinforced brittle-matrix composites*, Acta Metallurgica et Materialla, Vol. 41 no. 6, p1825-1839

12. W. Lee, W., Howard, S.J., and Cleg, W.J., 1996, *Growth of interface defects and its effect on crack deflection and toughening criteria*, Acta Metallurgica et Materialla 44 no 10, 3905-3922

13. Shukla, A., and Khanna, S.K., 1991, *Effect of fiber-matrix interface on toughening mechanisms during dynamic fracture of fiber reinforced materials*, ASME AMD - vol 130, Experiments in Micromechanics of failure resistant materials, 91-103

14. Mower, T.M., Argon, A.S., 1995, *Experimental investigations of crack trapping in brittle heterogeneous solids*, Mechanics of Materials, Vol. 19 p343-364

15. Theocaris, P.S., and Milos, J., 1981, *The process of the momentary arrest of a moving crack approaching a material discontinuity*, International Journal of Mechanical Science, vol 23 no 7, 423-436

16. Theocaris, P.S. and Demakos, C.B., 1988, *Crack propagation modes in particulates: A study approaching reality*, Journal of Composite Materials vol 22, 154-176

17. Griffith, A.A., 1920, Transactions of the Royal Society of London A, 221, p163-p182

18. Irwin, G.R., 1948, Fracture Dynamics, Fracturing of Metals, American Society for Metals, Cleveland, p147-166

19. Irwin, G.R., 1961, *Plastic zone near a crack and fracture toughness*, Sagamore Research Conference Proceedings, Vol. 4

20. Barenblatt, G.I., 1959, *The formation of equilibrium cracks during brittle fracture. General ideas and hypothesis. Axially symmetric cracks.*, Journal of Applied Mathematics and Mechanics, Vol 23 no. 3 p622-636

21. Barenblatt, G.I., 1962, Advances in Applied Mech, edit Dryden, H.L., vonKarmen, T., Academic Press, New York, p55-129

22. Dugdale, D.S., 1960, *Yielding in steel sheets containing slits*, Journal of the Mechanics and Physics of Solids, Vol 8 p100-104

23. Rose, L.R.F., 1987, *Crack Reinforcement by Distributed Springs*, Journal of the Mechanics and Physics of Solids, Vol. 35 no. 4 p383-405

24. Marshall, D.B., Cox, B.N. and Evans, A.G., 1985, *The mechanics of matrix cracking in brittle-matrix fiber composites*, Acta Metallurgica et Materialla, Vol. 33 p2013-2021

25. Budiansky, B., Hutchinson, J.W. and Evans, A.G., 1986, Journal of the Mechanics and Physics of Solids, Vol. 34, p 167-181

26. Eshelby, J.D., 1957, *The determination of the elastic field of an ellipsoidal inclusion, and related problems*, Proceedings of the Royal Society of London Ser. A, vol. 241, p 376-396

27. Bilby, B.A., Eshelby, J.D., Fracture, Edited by H. Liebowitz, 1968, Chapter 2, Academic Press, New York

28. Lange, F.F., 1970, *The Interaction of a Crack Front with a Second-phase Dispersion*, Philosophy Magazine, Vol. 22, p983-992

29. Evans, A.G.,1972, Philosophy Magazine, Ser. A, Vol. 26, 1327-1344

30. Green, D.J., Nicholson, P., Embury, J.D., 1979, *Fracture of a brittle particulate composite Part 1 Experimental aspects*, Journal of Material Science, Vol. 14 pp 1413-1420

31. Green, D.J., Nicholson, P., Embury, J.D., 1979, *Fracture of a brittle particulate composite Part 2 Theoretical aspects*, Journal of Material Science, Vol 14, pp 1657-1661

32. Rice, J.R., Cotterell, B., 1980, *Slightly curved or kinked cracks*, International Journal of Fracture, Vol. 16 p155-169

33. Rice, J.R., 1985a, *First order variations in elastic fields due to variation in location of a planar crack front*, Journal of Applied Mechancis, Vol. 52 p571-579

34. Rose, L.R.F., 1987, *Toughening due to crack-front interaction with a second phase dispersion*, Mechanics of Materials, Vol. 6 p11-15

35. Fares, N., 1989, *Crack fronts trapped by arrays of obstacles: numerical solutions based on surface integral representaion*, Journal of Applied Mechanics., Vol. 56 p837-843

36. Bower, A.F., Ortiz, M., 1990, *Solution of three-dimensional crack problems by a finite perturbation method*, Journal of the Mechanics and Physics of Solids, Vol. 38 no. 4 p443-480

37. Erdogan, F., Gupta, G.D., Ratwani, M., 1974, *Interaction between a circular inclusion and an arbitrarily oriented crack*, Journal of Applied Mechanics, December p1007-1013

38. Dekkers, M.E., Heikens, D., 1983, *The effect of interfacial adhesion on the mechanism for craze formation in polystyrene-glass bead composites*, Journal of Material Science, Vol. 18 p3281-3287

39. Evans, A.G., Hutchinson, J.W. , Dalgleish, B.J., He, M., 1989, *On crack path selection and the interface fracture energy in bimaterial systems*, Acta Metallurgica et Materialla, Vol. 3 p3248-3254

40. Lefebvre, J.M., Gerard, J.F., Amdouni, N., Fernagut, F., Coulon, G., 1990, *Coated glass beads epoxy composites: influence of the interlayer thickness on pre-yielding and fracture properties*, Journal of Material Science, Vol. 25 p1435-1443

41. Lee, W., Howard, S.J., Clegg, W.J., 1996, *Growth of interface defects and its effect on crack deflection and toughening criteria*, Acta Metallurgica et Materialla, Vol. 44 p3905-3922

42. Sanford, R.J., Dally, J.W., 1979, *A general method for determining mixed-mode stress intensity factors from isochromatic fringe patterns*, Enginering Fracture Mechanics, Vol. 11 p621-633

43. Irwin, G.R., 1980, *Series representation of the stress field around constant speed cracks*, University of Maryland lecture notes

44. Eshelby, J.D., 1961, *Elastic inclusions and inhomogeneities*, Progress in solid mechanics, I.N. Sneddon and R. Hill, eds., North Holland Amsterdam

45. Moschovidis, Z.A., Mura, T., 1975, *Two-ellipsoidal inhomogeneities by the equivalent inclusion method*, Journal of Applied Mechanics, Vol. 47 p847-852

46. Xiao, Z.M., Pae, K.D, 1991, *The interaction between a penny-shaped crack and a spherical inhomogeneity in an infinite solid under uniaxial tension,* Acta Mechanica., Vol. 90 p91-104

47. Miyata, N. and Jinno, H., 1981, *Strength and fracture surface energy of phase-separated glasses,* Journal of Material Science, Vol. 16 p2205-2217

BIBLIOGRAPHY

Anderson, T.L., 1991, <u>Fracture mechanics fundamental and applications,</u> CRC Press Inc, Boca Raton, Florida

Agarwal, B.D., Broutman, L.J., 1990, <u>Analysis and performance of fiber composites,</u> John Wiley & Sons Inc, New York

Barenblatt, G.I., 1959, *The formation of equilibrium cracks during brittle fracture. General Ideas and hypothesis. Axially symmetric cracks.*, <u>Journal of Applied Mathematics and Mechanics,</u> Vol 23 no. 3 p622-636

Barenblatt, G.I., 1962, <u>Advances in Applied Mech,</u> edit Dryden, H.L., vonKarmen, T., Academic Press, New York, p55-129)

Bilby, B.A., Eshelby, J.D., <u>Fracture,</u> Edited by H. Liebowitz, 1968, Chapter 2, Academic Press, New York

Bower, A.F., Ortiz, M., 1991, *A three-dimensional analysis of crack trapping and bridging by tough particles,* <u>Journal of the Mechanics and Physics of Solids,</u> Vol. 39 no. 6 p815-858

Bower, A.F., Ortiz, M., 1993, *An analysis of crack trapping by residual stresses in brittle solids,* <u>Journal of Applied Mechanics,</u> Vol. 60 p175-182

Bower, A.F., Ortiz, M., 1990, *Solution of three-dimensional crack problems by a finite perturbation method,* <u>Journal of the Mechanics and Physics of Solids,</u> Vol. 38 no. 4 p443-480

Budiansky, B., Hutchinson, J.W. and Evans, A.G., 1986, <u>Journal of Mechanics and Physics of Solids,</u> Vol. 34, p 167-181

Cox, B.N., Marshall, B.N., 1994, *Concepts for bridged cracks in fracture and fatigue,* <u>Acta Metallurgica et Materillia,</u> Vol. 42 no. 2 p341-363

Dekkers, M.E., Heikens, D., 1983, *The effect of interfacial adhesion on the mechanism for craze formation in polystyrene-glass bead composites,* <u>Journal of Material Science,</u> Vol. 18 p3281-3287

Dugdale, D.S., 1960, *Yielding in steel sheets containing slits,* <u>Journal of the Mechanics and Physics of Solids,</u> Vol 8 p100-104

Erdogan, F., Gupta, G.D., Ratwani, M., 1974, *Interaction between a circular inclusion and an arbitrarily oriented crack,* <u>Journal of Applied Mechanics,</u> December p1007-1013

Eshelby, J.D., 1957, *The determination of the elastic field of an ellipsoidal inclusion, and related problems,* <u>Proceedings of the Royal Society of London</u> Ser. A, vol. 241, p 376-396

Eshelby, J.D., 1961, *Elastic inclusions and inhomogeneities,* Progress in solid mechanics, I.N. Sneddon and R. Hill, eds., North Holland Amsterdam

Evans, A.G.,1972, Philosophy Magazine, Ser. A, Vol. 26, 1327-1344

Evans, A.G., Hutchinson, J.W. , Dalgleish, B.J., He, M., 1989, *On crack path selection and the interface fracture energy in bimaterial systems*, Acta Metallurgica et Materialla, Vol. 3 p3248-3254

Evans, A.G., Budiansky, B., Amazigo, J.C., 1988, *Small-scale crack bridging and the fracture toughness of particulate-reinforced ceramics*, Journal of the Mechanics and Physics of Solids,Vol. 36 no. 2 p167-187

Evans, A.G., Faber, K.T.,1983, *Crack deflection Processes: I Theory*, Acta Metallurgica et Materialla, Vol. 31 no. 4, p565-576

Evans, A.G., Faber, K.T.,1983, *Crack deflection Processes: II Experiment*, Acta Metallurgica et Materialla, Vol. 31 no. 4, p577-589,

Fares, N., 1989, *Crack fronts trapped by arrays of obstacles: numerical solutions based on surface integral representaion*, Journal of Applied Mechanics, Vol. 56 p837-843

Green, D.J., Nicholson, P., Embury, J.D., 1979, *Fracture of a brittle particulate composite Part 1 Experimental aspects*, Journal of Material Science, Vol. 14 pp 1413-1420

Green, D.J., Nicholson, P., Embury, J.D., 1979, *Fracture of a brittle particulate composite Part 2 Theoretical aspects*, Journal of Material Science, Vol 14, pp 1657-1661Vol. 31 no. 4, p577-584

Griffith, A.A., 1920, Philosophical Transactions Royal Society of London A, 221, p163-

Irwin, G.R., 1948, Fracture Dynamics, Fracturing of Metals, American Society for Metals, Cleveland, p147-166

Irwin, G.R., 1961, *Plastic zone near a crack and fracture toughness*, Sagamore Research Conference Proceedings, Vol. 4

Irwin, G.R., 1980, *Series representation of the stress field around constant speed cracks*, University of Maryland lecture notes

Lange, F.F., 1970, *The Interaction of a Crack Front with a Second-phase Dispersion*, Philosophy Magazine, Vol. 22, p983-992

Lee, W., Howard, S.J., and Cleg, W.J., 1996, *Growth of interface defects and its effect on crack deflection and toughening criteria*, Acta Metallurgica et Materialla 44 no 10, 3905-3922

Lefebvre, J.M., Gerard, J.F., Amdouni, N., Fernagut, F., Coulon, G., 1990, *Coated glass beads epoxy composites: influence of the interlayer thickness on pre-yielding and fracture properties*, Journal of Material Science, Vol. 25 p1435-1443

Marshall, D.B., Cox, B.N. and Evans, A.G., 1985, *The mechanics of matrix cracking in brittle-matrix fiber composites*, Acta Metallurgica et Materialla, Vol. 33 p2013-2021

Miyata, N. and Jinno, H., 1981, *Strength and fracture surface energy of phase-separated glasses*, Journal of Material Science, Vol. 16 p2205-2217

Moschovidis, Z.A., Mura, T., 1975, *Two-ellipsoidal inhomogeneities by the equivalent inclusion method*, Journal of Applied Mechanics, Vol. 47 p847-852

Mower, T.M., Argon, A.S., 1995, *Experimental investigations of crack trapping in brittle heterogeneous solids*, Mechanics of Materials, Vol. 19 p343-364

Pezzotti, G., 1993, *On the actual contribution of crack deflection in toughening platelet-reinforced brittle-matrix composites*, Acta Metallurgica et Materialla, Vol. 41 no. 6, p1825-1839

Pezzoti, G., Okamoto, Y., Nishida, T., Sakai, M., 1996, *On the near-tip toughening by crack-face bridging in particulate and platelet-reinforced ceramics*, Acta Metallurgica et Materialla Vol. 44 no. 3, p899-914

Rice, J.R., Gao, H., 1989, *A first-order perturbation analysis of crack trapping by arrays of obstacles*, Journal of Applied Mechanics, Vol. 56 pp 828-836

Rice, J.R., Cotterell, B., 1980, *Slightly curved or kinked cracks*, International Journal of Fracture, Vol. 16 p155-169

Rice, J.R., 1985a, *First order variations in elastic fields due to variation in location of a planar crack front*, Journal of Applied Mechanics, Vol. 52 p571-579

Rose, L.R.F., 1987, *Crack Reinforcement by Distributed Springs*, Journal of the Mechanics and Physics of Solids, Vol. 35 no. 4 p383-405

Rose, L.R.F., 1987, *Toughening due to crack-front interaction with a second phase dispersion*, Mechanics of Materials, Vol. 6 p11-15

Sanford, R.J., Dally, J.W., 1979, *A general method for determining mixed-mode stress intensity factors from isochromatic fringe patterns*, Engineering Fracture Mechanics, Vol. 11 p621-633

Shukla, A., and Khanna, S.K., 1991, *Effect of fiber-matrix interface on toughening mechanisms during dynamic fracture of fiber reinforced materials*, ASME AMD - vol 130 Experiments in Micromechanics of Failure Resistant Materials, 91-103

Theocaris, P.S., and Milos, J., 1981, *The process of the momentary arrest of a moving crack approaching a material discontinuity*, International Journal of Mechanical Science vol 23 no 7, 423-436

Theocaris, P.S., and Demakos, C.B., 1988, *Crack propagation modes in particulates: A study approaching reality*, J. of Composite Materials vol 22, 154-176

Xiao, Z.M., Pae, K.D, 1991, *The interaction between a penny-shaped crack and a spherical inhomogeneity in an infinite solid under uniaxial tension*, Acta Mechanica, Vol. 90 p91-104